Climate
of the Past

Summer temperature evolution on the Kamchatka Peninsula, Russian Far East, during the past 20 000 years

Vera D. Meyer[1,2], Jens Hefter[1], Gerrit Lohmann[1], Lars Max[1], Ralf Tiedemann[1], and Gesine Mollenhauer[1,2,3]

[1]Alfred Wegener Institute Helmholtz Centre for Polar and Marine Research, Bremerhaven, 27570, Germany
[2]Department of Geosciences University of Bremen, Bremen, 28359, Germany
[3]MARUM – Centre for Environmental Sciences, University of Bremen, Bremen, 28359, Germany

Correspondence to: Vera D. Meyer (vera.meyer@awi.de)

Abstract. Little is known about the climate evolution on the Kamchatka Peninsula during the last glacial–interglacial transition as existing climate records do not reach beyond 12 ka BP. In this study, a summer temperature record for the past 20 kyr is presented. Branched glycerol dialkyl glycerol tetraethers, terrigenous biomarkers suitable for continental air temperature reconstructions, were analyzed in a sediment core from the western continental margin off Kamchatka in the marginal northwest Pacific (NW Pacific). The record suggests that summer temperatures on Kamchatka during the Last Glacial Maximum (LGM) equaled modern temperatures. We suggest that strong southerly winds associated with a pronounced North Pacific High pressure system over the subarctic NW Pacific accounted for the warm conditions. A comparison with an Earth system model reveals discrepancies between model and proxy-based reconstructions for the LGM temperature and atmospheric circulation in the NW Pacific realm. The deglacial temperature development is characterized by abrupt millennial-scale temperature oscillations. The Bølling–Allerød warm phase and the Younger Dryas cold spell are pronounced events, suggesting a connection to North Atlantic climate variability.

1   Introduction

During the Last Glacial Maximum (LGM; i.e., 24–18 ka BP; Mix et al., 2001), when sea-level regression lead to the exposure of the Bering and Chukchi shelves, the Bering Land Bridge connected Alaska and eastern Siberia (Fig. 1). The resulting continuous landmass is commonly known as "Beringia" (defined as the area extending from the Lena River in northeastern Russia to the lower Mackenzie River in Canada; Hopkins et al., 1982). Beringia's environmental history since the last glaciation is of particular interest since having been unglaciated during the LGM, the landmass formed a glacial refuge for arctic flora and fauna (Abbott und Brochmann, 2003; Nimis et al., 1998; Guthrie, 2001) and allowed plants, animals and humans to migrate between Asia and North America (e.g., Mason et al., 2001). Despite several studies investigating the Beringian evolution of temperature, moisture availability and vegetation (e.g., Lozhkin et al., 1993, 2007; Anderson et al., 1996; Bigelow and Edwards, 2001; Bigelow and Powers, 2001; Pisaric et al., 2001; Elias, 2001; Ager, 2003; Kienast et al., 2005; Sher et al., 2005; Kurek et al., 2009; Elias and Crocker, 2008; Kokorowski et al., 2008a, b; Berman et al., 2011; Fritz et al., 2012; Anderson and Lozhkin, 2015), environmental change during the LGM-to-Holocene transition and the respective climatic controls (e.g., rising atmospheric CO_2 levels, insolation, and regional atmospheric and oceanic circulation) remain elusive. This is because continuous terrestrial records covering the entire last glacial–interglacial transition are sparse, particularly in western Beringia (i.e., Siberia; e.g., Kokorowski et al., 2008b, and references therein; Andreev et al., 2012; Anderson and Lozhkin, 2015). This is a gap of knowledge as independent terrestrial data on temperature and moisture availability are needed to infer LGM-to-Holocene changes in atmospheric circulation in the northern Pacific realm (e.g., Mock et al., 1998; Kokorowski et al., 2008b) and to validate climate model outputs.
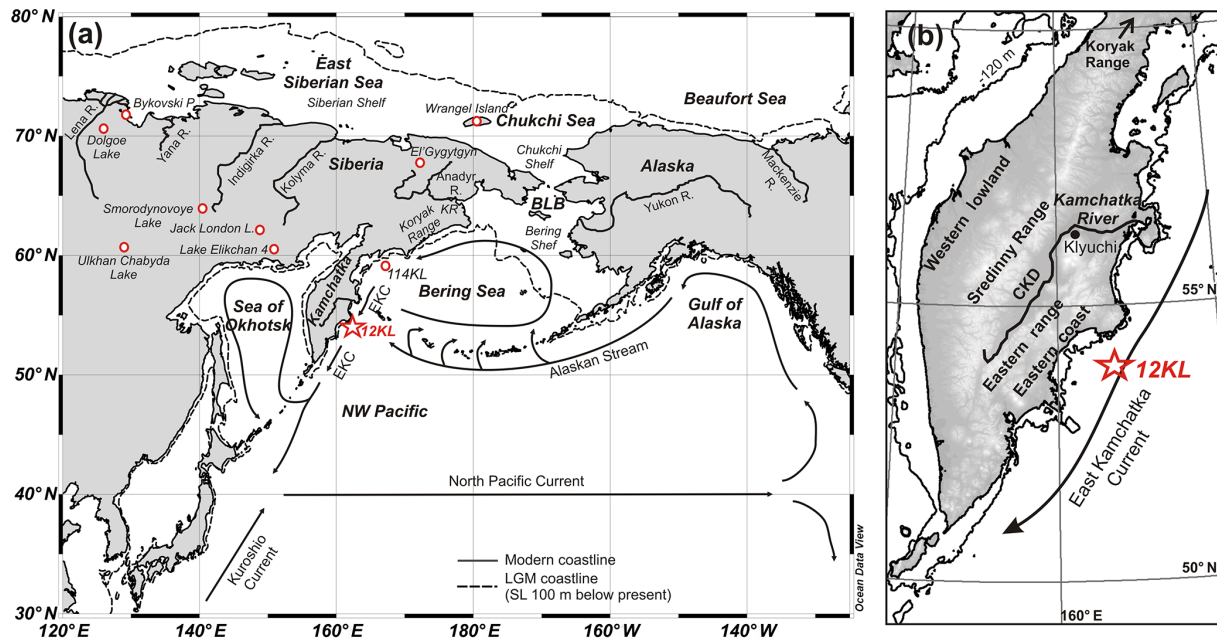
Figure 1. (a) Overview of Beringia and the N Pacific. Site SO201-2-12KL is marked by a red star. Circles represent sites mentioned in the text. Black arrows indicate the surface circulation patterns of the N Pacific (e.g., Stabeno and Reed, 1994). BLB is Bering Land Bridge, KR is Kankaren Range, R is river, EKC is East Kamchatka Current, P is peninsula and L is lake. **(b)** Map of the Kamchatka Peninsula and its major orographic units. CKD is Central Kamchatka Depression.

The sparsity of continuous temperature records in Beringia also limits a comprehensive assessment of the geographic extent of abrupt deglacial climate reversals. There is consensus among sea surface temperature records from the northern Pacific (N Pacific) and its marginal seas that the deglaciation was characterized by abrupt warm–cold oscillations (e.g., Barron et al., 2003; Seki et al., 2009, 2014; Caissie et al., 2010; Max et al., 2012; Praetorius and Mix, 2014; Praetorius et al., 2015; Meyer et al., 2016), suggesting teleconnections with the North Atlantic realm (Manabe and Stouffer, 1988; Mikolajewicz et al., 1997; Okumura et al., 2009; Chikamoto et al., 2012). However, it is not fully understood how far this North Atlantic (N Atlantic) connection extended into Beringia. Records are inconsistent, suggesting both abrupt warm–cold oscillations (Anderson et al., 1990, 2002; Andreev et al., 1997; Pisaric et al., 2001; Bigelow and Edwards, 2001; Bigelow and Powers, 2001; Brubaker et al., 2001; Meyer et al., 2010; Anderson and Lozhkin, 2015) and continuous warming (Lozhkin et al., 1993, 2001; Anderson et al., 1996, 2002, 2003; Lozhkin and Anderson, 1996; Bigelow and Powers, 2001; Nowaczyk et al., 2002; Ager, 2003; Nolan et al., 2003; Kokorowski et al., 2008a, b; Kurek et al., 2009) throughout the deglaciation.

The Kamchatka Peninsula (attached to Siberia, Fig. 1a) is among the areas in western Beringia where the least is known about environmental conditions during the LGM-to-Holocene transition since terrestrial archives on Kamchatka do not reach beyond 12 ka BP (e.g., Dirksen et al., 2013,

2015; Nazarova et al., 2013; Hoff et al., 2014, 2015; Klimaschewski et al., 2015; Self et al., 2015; Solovieva et al., 2015). Kamchatka is an important location to study deglacial changes in regional atmospheric and oceanic circulation in the northwestern Pacific realm. Protruding into the northwestern Pacific (NW Pacific, Fig. 1a), the peninsula responds to variations in these regional climate controls in addition to global or supraregional climate drivers, e.g., summer insolation or teleconnections with the N Atlantic realm, as has been shown for the Holocene (Savoskul, 1999; Dirksen et al., 2013; Nazarova et al., 2013; Andrén et al., 2015; Brooks et al., 2015; Hammarlund et al., 2015; Self et al., 2015).

In this study, we analyzed branched glycerol dialkyl glycerol tetraethers (brGDGTs), terrigenous biomarkers as recorders of continental air temperature (Weijers et al., 2006a, 2007), in a marine sediment core retrieved at the eastern continental margin off Kamchatka and the NW Pacific (site SO201-2-12KL, NW Pacific; Fig. 1a, b). We present a continuous, quantitative record of summer temperature for the past 20 kyr and infer changes in atmospheric circulation. The findings are compared to an Earth system model (ESM).

2   Regional setting

The Kamchatka Peninsula is situated south of the Koryak Uplands and separates the Sea of Okhotsk from the NW Pacific and the Bering Sea (Fig. 1a). It is characterized by strong variations in relief with lowlands in the coastal areas

(western lowlands and eastern coast) and mountain ranges further inland (Fig. 1b). The mountain ranges, the Sredinny and the eastern ranges, encircle the lowlands of the Central Kamchatka Depression (CKD, Fig. 1b). The CKD is the largest watershed of the peninsula and is drained by the Kamchatka River, the largest river of Kamchatka. The river discharges into the Bering Sea near 56° N (Fig. 1b). The climate is determined by marine influences from the surrounding seas, by the east Asian continent, and by the interplay between the major atmospheric pressure systems over NE Asia and the N Pacific (e.g., Mock et al., 1998; Glebova et al., 2009). In general, the climate is classified as subarctic maritime (Dirksen et al., 2013). The winters are characterized by cold and relatively continental conditions since northerly winds prevail over Kamchatka, mainly associated with the Aleutian Low over the N Pacific and the Siberian High over the continent (Mock et al., 1998). In summer, Kamchatka experiences warm maritime conditions owing to the East Asian Low over the continent and the North Pacific High (NPH) over the N Pacific (Mock et al., 1998). Furthermore, there are the influences of the East Asian Trough, which has its average position over the Chukchi Shelf, as well as the influences of the westerly jet stream and the associated polar front (Mock et al., 1998). Variations in the position and strength of the East Asian Trough affect precipitation and temperature over Beringia and can cause climatic contrasts between Siberia and Alaska (Mock et al., 1998, and references therein). With respect to Kamchatka, westerly to northwesterly winds associated with the jet stream and the East Asian Trough form a source of continental air masses from Siberia to eastern Asia (Mock et al., 1998).

The mountainous terrain with strongly variable relief results in pronounced climatic diversity on the peninsula (Fig. 1b). The coastal areas, the western lowlands and the eastern coast are dominated by marine influences. In the coastal areas, summers are cool and wet and winters are relatively mild. Precipitation is high along the coast and in the mountains throughout the year (Kondratyuk, 1974; Dirksen et al., 2013). Being protected from marine influences by the mountain ranges, the CKD has more continental conditions with less precipitation and a larger annual temperature range than in the coastal areas (Ivanov, 2002; Dirksen et al., 2013; Kondratyuk, 1974; Jones and Solomina, 2015). Mean temperatures averaged for the entire peninsula range from -8 to $-26\,°C$ in January and from 10 to 15 °C in July (Ivanov, 2002).

3 Material and methods

3.1 Core material and chronology

Within a joint German–Russian research program (KALMAR Leg 2), core SO201-2-12KL (Fig. 1a, b) was recovered with a piston-corer device during cruise R/V *Sonne* SO201 in 2009 (Dullo et al., 2009). The core material

was stored at 4 °C prior to sample preparation. Age control is based on accelerator mass spectrometry (AMS) radiocarbon dating of planktic foraminifera (*Neogloboquadrina pachyderma* sin., nine dates in total) as well as on correlations of high-resolution spectrophotometric (color b*) and X-ray fluorescence (XRF) data from different sediment cores from the NW Pacific, the Bering Sea and the Sea of Okhotsk (Max et al., 2012). The correlation allowed the transfer of AMS results from core to core, which provided 10 additional age control points for site 12KL (Max et al., 2012). Max et al. (2012) converted radiocarbon ages into calibrated calendar ages using the calibration software CALIB Rev 6.0 (Stuiver and Reimer, 1993) with the Intcal09 atmospheric calibration curve (Reimer et al., 2009). A constant reservoir age of 900 years was assumed for the entire time interval covered by the core. The uncertainty of AMS dating was smaller than ±100 years (Max et al., 2012). Another important source of uncertainty are changes in reservoir ages of the surface ocean during the last deglaciation (Sarnthein et al., 2015). However, recent studies suggest that reservoir ages of the Bering Sea and the N Pacific varied by less than 200 years (Lund et al., 2011; Kuehn et al., 2014) and are within the range of reservoir ages originally assumed by Max et al. (2012).

Average Holocene, deglacial and glacial sedimentation rates are 39, 79 and 59 cm ka^{-1}, respectively, allowing for climate reconstructions on multi-centennial to millennial timescales (Max et al., 2012). For more detailed information about the stratigraphic framework and AMS ^{14}C results, see Max et al. (2012).

3.2 Lipid extraction

For this study we used the same samples as Meyer et al. (2016). These authors sampled the core in 10 cm steps, providing an average temporal resolution of approximately 200 years. For GDGT (glycerol dialkyl glycerol tetraether) analyses, freeze-dried and homogenized sediment samples (approximately 5 g) were extracted and processed according to Meyer et al. (2016).

3.3 GDGT analysis

GDGTs were analyzed by high-performance liquid chromatography (HPLC) and a single quadrupole mass spectrometer (MS). The systems were coupled via an atmospheric pressure chemical ionization (APCI) interface. The applied method was slightly modified from Hopmans et al. (2000). Analyses were performed on an Agilent 1200 series HPLC system and an Agilent 6120 mass selective detector (MSD). Separation of the individual GDGTs was performed on a Prevail Cyano column (Grace, 3 µm, 150 mm × 2.1 mm), which was maintained at 30 °C. After sample injection (20 µL) and 5 min isocratic elution with solvents A (hexane) and B (hexane with 5 % isopropanol) at a mixing ratio of 80 : 20,

the proportion of B was increased linearly to 36 % within 40 min. The eluent flow was $0.2 \, \text{mL min}^{-1}$. After each sample, the column was cleaned by back-flushing with 100 % solvent B (8 min) and re-equilibrated with solvent A (12 min, flow $0.4 \, \text{mL min}^{-1}$). GDGTs were detected using positive-ion APCI–MS and selective ion monitoring (SIM) of their $(M + H)^+$ ions (Schouten et al., 2007). APCI spray-chamber conditions were set as follows: nebulizer pressure at 50 psi, vaporizer temperature at 350 °C, N_2 drying gas flow at $5 \, \text{L min}^{-1}$ and 350 °C, capillary voltage (ion transfer tube) at $-4 \, \text{kV}$ and corona current at $+5 \, \mu\text{A}$. The MS detector was set in SIM mode, detecting the following $(M + H)^+$ ions with a dwell time of 67 ms per ion: m/z 1292.3 (GDGT $4 + 4'$/crenarcheol + regioisomer), 1050 (GDGT IIIa), 1048 (GDGT IIIb), 1046 (GDGT IIIc), 1036 (GDGT IIa), 1034 (GDGT IIb), 1032 (GDGT IIc), 1022 (GDGT Ia), 1020 (GDGT Ib), 1018 (GDGT Ic) and 744 (C_{46} internal standard).

GDGTs were quantified by peak integration and the obtained response factor from the C_{46} standard. Concentrations were normalized to the dry weight (dw) of the extracted sediment and to total organic carbon contents (TOC). It has to be noted that the quantification should only be regarded as semi-quantitative because individual relative response factors between the C_{46} standard and the different brGDGTs could not be determined due to the lack of appropriate standards. Fractional abundances of single brGDGTs were calculated relative to the total abundance of all nine brGDGTs. The standard deviation was determined from repeated measurements of a lab internal standard sediment and resulted in an uncertainty of 9 % for the concentration of the sum of all nine brGDGTs (ΣbrGDGT).

3.4 Temperature determination

The Cyclisation of Branched Tetraethers index (CBT) and Methylation of Branched Tetraether index (MBT) were introduced as proxies for soil pH (CBT) and mean annual air temperature (MAT, CBT–MBT) by Weijers et al. (2007). We calculated the CBT index after Weijers et al. (2007). For calculating the MBT index we used a modified version, the MBT', which excludes GDGTs IIIb and IIIc and was introduced by Peterse et al. (2012). From repeated measurements of a lab internal standard sediment extract ($n = 7$), the standard deviation for CBT and MBT' were determined as 0.01 and 0.04, respectively. CBT and MBT' values were converted into temperature using the global soil dataset calibration by Peterse et al. (2012). The residual standard mean error of this calibration is 5 °C (Peterse et al., 2012). The standard deviation of CBT and MBT' translates into an uncertainty of maximum 0.1 °C.

Although terrestrial soils are supposed to be the main source of brGDGTs (Weijers et al., 2007), brGDGT can also be produced in situ in marine water systems (Peterse et al., 2009; Zhu et al., 2011; Zell et al., 2014) as well as in fresh-

water environments (Tierney et al., 2010; Zell et al., 2013; De Jonge et al., 2014; Dong et al., 2015). As in situ production can bias temperature reconstructions, particularly in marine settings where the input of terrigenous GDGTs is low (Weijers et al., 2006b; Peterse et al., 2009, 2014; De Jonge et al., 2014), the contribution of terrigenous brGDGTs to the marine sediments needs to be estimated prior to any paleoclimatic interpretation of temperatures derived from CBT–MBT'. A common means to estimate the relative input of marine and terrestrial GDGTs is the BIT index (branched and isoprenoid tetraether index), which quantifies the relative contribution of the marine-derived crenarchaeol and terrigenous brGDGTs (Hopmans et al., 2004). The higher the BIT value, the more abundant the brGDGT relative to the crenarchaeol and the higher the terrigenous input. BIT values were adopted from Meyer et al. (2016), who worked on the same samples as used in this study.

3.5 Climate simulations with the Earth system model COSMOS

In order to compare inferences for atmospheric circulation during the summer months to general circulation model outputs, model simulations for the climate were performed with the ESM COSMOS for preindustrial (PI) (Wei et al., 2012) and LGM conditions (Zhang et al., 2013). The model configuration includes the atmosphere component ECHAM5 at T31 resolution ($\sim 3.75°$) with 19 vertical layers (Roeckner et al., 2006), complemented by a land-surface scheme, including dynamical vegetation (Brovkin et al., 2009). The ocean component MPI-OM, including the dynamics of sea ice formulated using viscous-plastic rheology, has an average horizontal resolution of $3° \times 1.8°$ with 40 uneven vertical layers (Marsland et al., 2003). The performance of this climate model was evaluated for the Holocene (Wei and Lohmann, 2012; Lohmann et al., 2013), the last millennium (Jungclaus et al., 2006), glacial millennial-scale variability (Gong et al., 2013; Weber et al., 2014; Zhang et al., 2014), and warm climates in the Miocene (Knorr and Lohmann, 2014) and Pliocene (Stepanek and Lohmann, 2012).

External forcing and boundary conditions are imposed according to the protocol of PMIP3 for the LGM (available at http://pmip3.lsce.ipsl.fr/). The respective boundary conditions for the LGM comprise orbital forcing, greenhouse gas concentrations ($CO_2 = 185$ ppm, $N_2O = 200$ ppb, $CH_4 = 350$ ppb), ocean bathymetry, land surface topography, run-off routes according to PMIP3 ice sheet reconstruction and increased global salinity ($+1$ psu compared to modern values) to account for a seal level drop of ~ 116 m. The glacial ocean was generated through an ocean-only phase of 3000 years and a coupled phase of 3000 years (LGMW in Zhang et al., 2013). The land cover is calculated interactively in the climate model, which has an interactive land surface scheme and vegetation module (Brovkin et al., 2009). The modular land surface scheme JSBACH (Raddatz et al.,
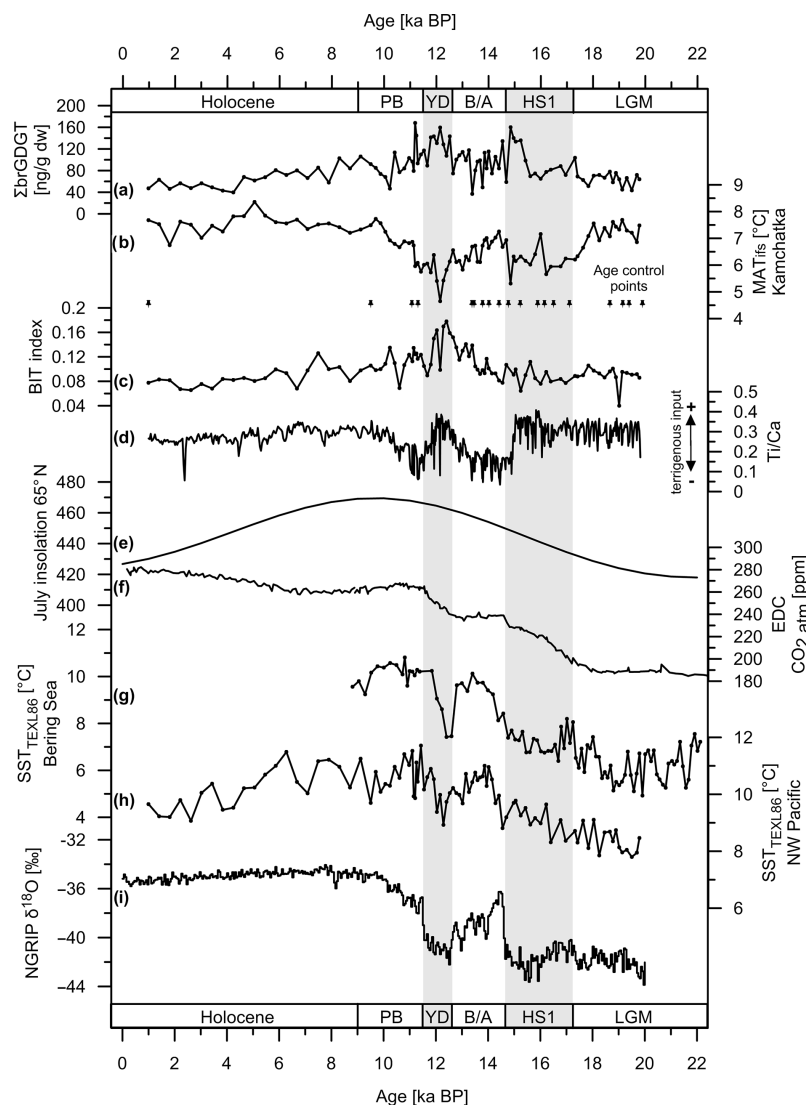
Figure 2. (a) Concentrations of ΣbrGDGT of core 12KL. **(b)** MAT$_{ifs}$ derived from CBT–MBT′ from Kamchatka (this study). Black pins represent the age control points from core 12KL (based on radiocarbon dating of planktonic foraminifera; Max et al., 2012). **(c)** BIT index values of core 12KL (Meyer et al., 2016). **(d)** Titanium / calcium ratios (Ti / Ca, XRF-scan core 12KL; Max et al., 2012). **(e)** Mean July insolation at 65° N (Berger and Loutre, 1991). **(f)** Atmospheric CO_2 concentration (EPICA dome C; Monnin et al., 2001; Parrenin et al., 2013). **(g)** SST development in the marginal NW Pacific (site 12KL; Meyer et al., 2016). **(h)** SST evolution in the western Bering Sea (site 114KL; Meyer et al., 2016). **(i)** NGRIP δ^{18}O (NGRIP members, 2004) represents climate change in the N Atlantic. Grey shaded bars mark the HS1 and YD stadials.

2007) with vegetation dynamics (Brovkin et al., 2009) is embedded in the ECHAM5 atmosphere model. The background soil characteristics (which are described in Stärz et al., 2016) are set to the values that are closest to the PI land points.

For both, PI and LGM conditions the climate model was integrated twice for 3000 model years and provides monthly output (Wei et al., 2012; Wei and Lohmann, 2012; Zhang et al., 2013). Here, anomalies in sea-level pressure (SLP), wind directions (1000 hPa level) and surface air temperature (SAT) between the LGM and preindustrial conditions were analyzed for the boreal summer season – June, July and August

(JJA). We focus on the summer season as in high latitudes brGDGTs seem to reflect summer temperature instead of the annual mean (Rueda et al., 2009; Shanahan et al., 2013; Peterse et al., 2014). All produced figures show climatological mean characteristics averaged over a period of 100 years at the end of each simulation.
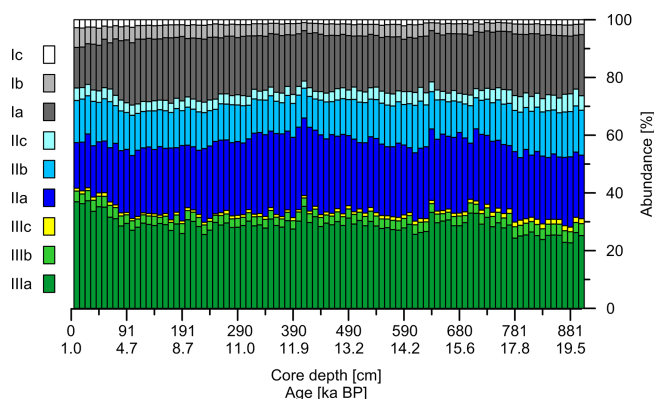
Figure 3. Fractional abundances of all nine brGDGT in core 12KL, given in percentage relative to the amount of ΣbrGDGTs.

4   Results

4.1   Concentrations and fractional abundances of brGDGTs

The summed concentration of all nine brGDGTs (ΣbrGDGT) is shown in Fig. 2a. The concentration of ΣbrGDGTs varies between 40 and 160 ng g^{-1} dw throughout the record. Ranging between 60 and 80 ng g^{-1} dw, they are lowest during the LGM and the late Holocene. During the deglaciation and the early Holocene (17–8 ka BP), lowest values are approximately 80 ng g^{-1} dw, except for two peaks at 15–16 and 12–13 ka BP where concentrations reach $\sim$ 160 ng g^{-1} dw (Fig. 2a).

The fractional abundance of all nine brGDGTs, calculated relative to the ΣbrGDGT, is shown in Fig. 3. All samples are characterized by a similar pattern. The composition of the brGDGT assemblage is dominated by brGDGTs without cyclopentyl moieties, which together account for 60–80 % of the total brGDGT assemblage (GDGT Ia, IIa, IIIa; Fig. 3). BrGDGTs with a higher degree of methylation are more abundant than less-methylated ones. In 88 out of 92 samples GDGT IIIa is the most prominent brGDGT, accounting for 22–37 % of the total brGDGT distribution. It is closely followed by GDGT IIa with 16–29 % and GDGT Ia, which accounts for 14–23 % of the total brGDGT assemblage. As for brGDGTs containing cyclopentyl moieties, GDGT IIb is most abundant, accounting for 9–16 % of the total brGDGT assemblage. GDGTs IIc, Ib, Ic, IIIb and IIIc are less abundant, reaching 2–6, 3–7, 1–3, 2–4 and 1–2, respectively (Fig. 3).

4.2   Temperature development over the past 20 kyr

The temperatures derived from CBT–MBT' are plotted in Fig. 2b. Glacial (20–18 ka BP) and late Holocene (1–3 ka BP) temperatures are similar ($\sim$ 7.5 °C) (Fig. 2b). The deglaciation is characterized by abrupt temperature variations. At 18 ka, temperature drops by $\sim$ 1.5 °C and remains relatively

cold until approximately 14.6 ka BP, when it abruptly jumps back to the glacial and Holocene level of $\sim$ 7.5 °C (Fig. 2e). Between $\sim$ 14.6 and $\sim$ 13 ka, temperature progressively decreases by $\sim$ 1–0.5 °C. Temperature abruptly decreases by $\sim$ 2 °C at approximately 13 ka BP and remains cold until 12 ka BP (Fig. 2b). The cold spell is followed by a sharp temperature increase of $\sim$ 3 °C at the onset of the pre-Boreal (PB) to the early Holocene (Fig. 2b). After the abrupt temperature increase into the PB, temperature progressively increases, culminating in a Mid-Holocene Thermal Maximum (HTM) between $\sim$ 8 and $\sim$ 4–5 ka BP, where temperatures ranges between $\sim$ 7.5 and 8 °C (Fig. 2b).

4.3   LGM climate simulation with COSMOS

4.3.1   Sea-level pressure and wind patterns

Model simulations for SLP (JJA) are shown Fig. 4a. The LGM simulation is characterized by strong positive anomalies in SLP over the North American continent (Fig. 4a). Positive SLP anomalies also occur over the Arctic Ocean. Negative SLP anomalies occur south of 50° N and are centered over the NW Pacific and eastern Asia, but they are also observed in a few grid cells over the central and northeastern (NE Pacific) and over the Sea of Okhotsk. In the Bering Sea, the northern N Pacific (north of 50° N) and Beringia SLP does not change significantly relative to PI SLP.

The positive SLP anomalies over North America are associated with pronounced anticyclonic anomalies in the wind directions, which expand to the Chukchi Sea and to the formerly exposed Bering Land Bridge (Fig. 4a). Over western Beringia as well as the adjacent Arctic Ocean, small northerly anomalies are present. Between 100 and 110° E, pronounced anticyclonic anomalies are present over Russia. Over Kamchatka and the adjacent eastern Siberian coast, small northerly anomalies occur. The western Bering Sea is characterized by easterly anomalies. Over the NW Pacific, anomalies are small and show no general pattern. In the NE Pacific relatively strong westerly to southwesterly anomalies are present.

4.3.2   Surface air temperature

Model simulations for SAT (JJA) are shown in Fig. 4b. The model predicts widespread negative SAT anomalies over Beringia, eastern Asia, North America, the Arctic Ocean and the entire N Pacific (Fig. 4b). However, in small parts of the formerly exposed Bering Land Bridge conditions that are slightly warmer than present occur. On the arctic shelf there is a small band where temperature is similar to the PI conditions (the SAT anomaly falls in the window of −1 to +1 °C). The temperature anomalies are strongest over North America where they reach −17 °C. Over western Beringia, the SAT anomaly becomes more pronounced from east to west, with SAT ranging between −1 and −5 over eastern Siberia and between −5 and −9 further west. Over the N Pacific, SAT
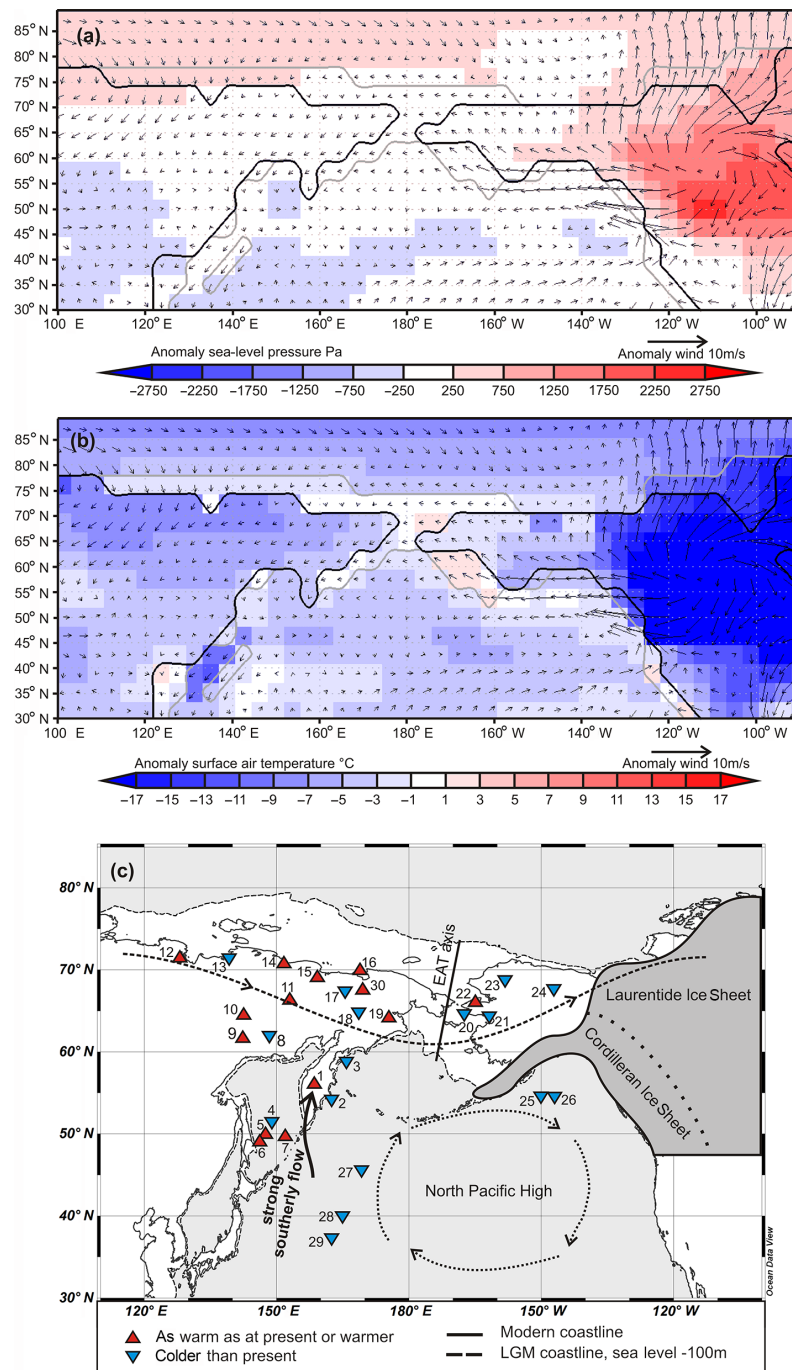
Figure 4. Comparison of proxy- and model-based inferences regarding glacial anomalies in temperature and atmospheric circulation over the N Pacific and Beringia relative to present. **(a)** COSMOS simulation for the JJA SLP anomaly over Beringia and the N Pacific during the LGM (21 ka) relative to PI. Arrows represent the wind anomaly. Note that the model predicts a northerly anomaly over Kamchatka. **(b)** COSMOS-simulation for SAT and wind anomalies during JJA. **(c)** Compilation of proxy-based anomalies of summer air temperature in Beringia and of summer–autumn SST reconstructions in the N Pacific for the LGM. Sites and corresponding references are given in the Appendix A. Dotted arrows sketch the general summer anticyclone over the N Pacific, the NPH. Based on MAT$_{ifs}$, the NPH and associated southerly winds over the subarctic NW Pacific were stronger than at present (represented by solid arrow). The dashed line marks the approximate average position of the East Asian Trough (EAT) during present day summers (Mock et al., 1998). Grey shaded areas represent the extent of ice sheets during the LGM.

anomalies are smaller than over western Beringia and range between −1 and −5 °C. SAT anomalies are smallest in the Bering Sea and along the eastern coast of Kamchatka. Over the peninsula itself, the majority of grid cells indicate a negative anomaly (−3 to −5 °C). In the northern part and over the adjacent Bering Sea, the SAT anomalies are very small, within the window of −1 to +1 °C (Fig. 4b).

5 Discussion

5.1 Sources of brGDGT and implications for temperatures derived from CBT–MBT′

Considering that brGDGTs are thought to be synthesized by terrestrial bacteria that thrive in peats and soils (e.g., Weijers et al., 2006b), it is most likely that the major origin of brGDGTs in the marine sediments of the Bering Sea and NW Pacific would be the Kamchatka Peninsula. However, BIT values from core 12KL range between 0.08 and 0.2 (Meyer et al., 2016) throughout the entire record, indicating that marine-derived GDGTs dominate the total GDGT composition and that terrigenous input is low (Fig. 2c). Marine settings where terrigenous input is low are particularly sensitive to bias from in situ production (e.g., Weijers et al., 2006b; Peterse et al., 2009; Zhu et al., 2011); thus, non-soil-derived brGDGTs potentially have a considerable effect on the temperature reconstruction at site 12KL. However, the concentrations of ΣbrGDGT shows similarities with the trend of titanium / calcium ratios (Ti / Ca ratios, Fig. 2d) from core 12KL (XRF data from Max et al., 2012). Ti / Ca ratios reflect the proportion of terrigenous and marine-derived inorganic components of the sediment and can be used as an estimator of terrigenous input. With relatively high values at 15.5 and 12 ka BP, and minima at 14 and 11 ka BP, Ti / Ca indicates relatively high contributions of terrigenous material relative to marine components at 15.5 and 12 ka BP and relatively low terrigenous contributions at 14 and 11 ka BP. A similar pattern is visible in ΣbrGDGT concentrations as these increase during intervals of enhanced terrigenous input (high Ti / Ca values) and decrease when terrigenous input is relatively low (low Ti / Ca values; see Fig. 2b, d). This suggests that brGDGTs are terrigenous. Moreover, the distribution of the brGDGTs in the samples from site 12KL resemble the brGDGT composition described for soils worldwide (Weijers et al., 2007; Blaga et al., 2010) as GDGT Ia, IIa and IIIa dominate over brGDGTs with cyclopentyl moieties (e.g., Ib, IIb), accounting for 60–80 % of the total brGDGT assemblage (Fig. 3). By contrast, in marine areas where brGDGTs are thought to be produced in situ, the brGDGT compositions were dominated by brGDGTs containing cyclopentyl moieties (Peterse et al., 2009; Zell et al., 2014). Thus, brGDGT seem to be soil-derived and a bias from in situ production is unlikely. We also exclude changes in the source of brGDGTs through time because the relative abundance of the brGDGTs is similar in all samples, indicating that the source of brGDGTs remained constant throughout the past 20 kyr (Fig. 3). We consider the catchment of the Kamchatka River (CKD and inner flanks of the mountains) and the eastern coast as the likely sources of brGDGTs deposited in the marine sediments at the core site since the Kamchatka River and several small rivers draining the eastern coast discharge into the western Bering Sea. Flowing southward along Kamchatka, the East Kamchatka Current would carry the load of the Kamchatka River to site 12KL (Fig. 1b)

Although the CBT–MBT paleothermometer has been suggested to generally record mean annual air temperatures (Weijers et al., 2007), it is assumed to be biased to the summer months and ice-free season in high latitudes (Rueda et al., 2009; Shanahan et al., 2013; Peterse et al., 2014). According to the Klyuchi climate station (for location see Fig. 1b), mean annual air temperatures in the northern CKD are −0.5 °C (Klyuchi climate station, http://en.climate-data.org/location/284590/, 2015). The temperatures derived from CBT–MBT′ for the core top, i.e., late Holocene (7.5 ± 5 °C; Fig. 2), exceed the annual mean by ∼ 8 °C and are similar to mean air temperatures from the ice-free season (May–October) at Klyuchi (9 °C). Therefore, they are interpreted as summer temperature and will henceforth be referred to as "mean air temperature of the ice-free season" (MAT$_{ifs}$).

5.2 Temperature evolution over the past 20 kyr

5.2.1 The LGM (until 18 ka)

The finding that LGM summers were as warm as during the Holocene contrasts with the general understanding of the glacial climate, according to which the extratropics were significantly colder than today, as documented by several proxy-based temperature reconstructions and general circulation model simulations (e.g., MARGO compilation or PIMP, and others; see Kutzbach et al., 1998; Kageyama et al., 2001, 2006; Kim et al., 2008; Waelbroeck et al., 2009; Braconnot et al., 2012; Alder and Hostetler, 2015). Generally cooler LGM temperatures are thought to result from low summer insolation, reduced carbon dioxide concentrations in the atmosphere and extensive continental ice sheets (Berger and Loutre, 1991; Monnin et al., 2001; Kageyama et al., 2006; Shakun et al., 2012). Therefore, one may expect that the Kamchatka Peninsula would experience a glacial–interglacial warming trend. As MAT$_{ifs}$ deviates from the trends in atmospheric CO_2 (CO_{2atm}) and insolation (Fig. 2b, e, f), regional climate drivers may have overprinted the effects of CO_{2atm} and summer insolation. Interestingly, several studies investigating climate in Beringia based on pollen and beetle assemblages indicate that in northeastern Siberia and the formerly exposed Bering Land Bridge (catchments of the Lena, Kolyma, and Indigirka rivers; Ayon Island; Anadyr lowlands; Lake El'Gygytgyn; Seward Peninsula; Fig. 4c) summers during the LGM were as warm as at present or were even warmer (Fig. 4c; Elias et al., 1996, 1997; Elias,

2001; Alfimov and Berman, 2001; Kienast, 2002; Kienast et al., 2005; Sher et al., 2005; Berman et al., 2011). Only a few pollen and insect data from Markovo, Jack London and Lake El'Gygytgyn lakes (Fig. 1a) point to colder-than-present summer conditions (Fig. 4c; Lozhkin et al., 1993, 2007; Alfimov and Bermann, 2001; Pitul'ko et al., 2007). The fairly large number of sites indicating warm summers in Siberia suggests that a thermal anomaly was widespread over western–central Beringia (Fig. 4c) and extended to Kamchatka. The thermal anomaly probably did not extend to eastern Beringia as insect data and pollen consistently point to summer cooling of up to 4 °C (Fig. 4c; e.g., Matthews Jr. and Telka, 1997; Elias, 2001; Kurek et al., 2009).

5.2.2 Regional control on MAT$_{ifs}$

In previous studies, the warm Siberian summers during the LGM were attributed to increased continentality, which would arise from the exposure of the extensive Siberian and Chukchi shelves at times of lowered sea level (Fig. 1a; e.g., Guthrie, 2001; Kienast et al., 2005; Berman et al., 2011). The greater northward extent of the Beringian landmass (approximately +800 km relative to today) would have minimized maritime influences from the cold Siberian and Chukchi seas (Guthrie, 2001; Alfimov and Berman, 2001; Kienast et al., 2005; Sher et al., 2005; Berman et al., 2011). Increased seasonal contrasts resulting in warmer summers and colder winters would have been the result (e.g., Guthrie, 2001; Kienast et al., 2005). Winter cooling in Siberia (relative to modern conditions) is indicated by ice-wedge data (Meyer et al., 2002) from the Bykovski Peninsula (Fig. 1a). Also, the presence of stronger-than-present sea-ice cover in the Bering Sea (Caissie et al., 2010; Smirnova et al., 2015) points to cold winters in Siberia and Kamchatka during the LGM. However, for Kamchatka it is unlikely that the thermal anomaly and an increased seasonal contrast were a direct result from lowered sea level as the bathymetry around the peninsula is relatively steep and the exposed shelf area was very small. (Fig. 1a, b). Thus, other climate drivers were likely responsible for the relatively warm summer conditions. Potential mechanisms are changes in oceanic or atmospheric circulation.

Intriguingly, $U_{37}^{K'}$-based SST reconstructions from the Sea of Okhotsk indicate that glacial SSTs were slightly warmer than today or equal to modern conditions (Seki et al., 2004, 2009; Harada et al., 2004, 2012; Fig. 4c). However, these records are considered to be biased by seasonal variations in the alkenone production rather than to reflect real temperature anomalies (Seki et al., 2004, 2009; Harada et al., 2004, 2012). This seems to be supported by a few TEX$_{86}^{L}$-based SST reconstructions from the Sea of Okhotsk, suggesting that LGM SSTs were ~ 5 °C colder than at present (Seki et al., 2009, 2014). In this light, a climatic relation between alkenone-based SST and MAT$_{ifs}$ seems very unlikely. Interestingly, LGM SSTs in the subarctic NW Pacific

(site 12KL, TEX$_{86}^{L}$) were only ~ 1 °C lower than at present (Fig. 2h), a relatively small temperature difference compared to other SST records from the NW Pacific and its marginal seas (all obtained from TEX$_{86}^{L}$), which suggest a cooling of ~ 4–5 °C (e.g., Seki et al., 2009, 2014; Meyer et al., 2016). The relatively warm SSTs at site 12KL were explained by a stronger-than-present influence of the Alaskan Stream in the marginal NW Pacific (Meyer et al., 2016). Such warm SSTs may have supported the establishment of warm conditions on Kamchatka. However, it is unlikely that the temperature development on Kamchatka was fully controlled by oceanic influences since this would probably have caused a reduction of LGM MAT$_{ifs}$ relative to present.

If oceanic circulation alone is unlikely to have caused the warm temperatures on Kamchatka, atmospheric circulation may have exerted an important control on glacial summer temperatures in the region. In terms of atmospheric circulation, the summer climate of Kamchatka is largely determined by the strength and position of the NPH over the N Pacific (Mock et al., 1998). As the southerly flow at the southwestern edge of the NPH brings warm and moist air masses to Kamchatka, summers on the peninsula become warmer when the NPH and the associated warm southerly flow increase in strength (Mock et al., 1998). This modern analogue suggests that the LGM NPH over the subarctic NW Pacific was stronger than today and the resulting warming effect may have balanced the cooling effects of CO$_{2atm}$ and insolation.

Comparison to the COSMOS simulations

These inferences contrast with results from the climate simulations with COSMOS. For JJA, the model predicts a decrease in SLP over the NW Pacific, suggesting that the southerly flow at the western edge of the NPH was reduced rather than strengthened (Fig. 4a). The weakening of the southerly flow is also discernable in the anomaly of the major wind patterns over the NW Pacific (Fig. 4a) as a small northerly anomaly occurs north of Kamchatka, over the peninsula itself and along the Asian coast (Fig. 4a). The weakening of the NPH is in agreement with several other general circulation models (GCMs), which consistently predict a reduction in SLP over the N Pacific (Kutzbach and Wright, 1985; Bartlein et al., 1998; Dong and Valdes, 1998; Vettoretti et al., 2000; Yanase and Abe-Ouchi, 2007; Alder and Hostetler, 2015). It has been suggested that a pronounced positive SLP anomaly and a persistent anticyclone over the North American continent resulted in reduced SLP over the western northern Pacific (Yanase and Abe Ouchi, 2010). The positive SLP anomaly and the strong anticyclonic tendencies are clearly present in the COSMOS simulation of SLP and wind patterns (Fig. 4a) and were also simulated by several other GCMs (e.g., Yanase and Abe-Ouchi, 2007, 2010; Alder and Hostetler, 2015). Its development was attributed to the presence of extensive ice sheets on the North American continent (Yanase and Abe-Ouchi, 2010), which would have

caused severe cooling of the overlying atmosphere. Considering the consistency of different GCMs, the anticyclonic anomalies over North America as well as resulting cyclonic anomalies over the N Pacific seem to be a robust feature of the glacial atmospheric circulation. Therefore, it is unlikely that the increased influence of the NPH over Kamchatka (as inferred from MAT_{ifs}) was caused by a general strengthening of the NPH. We hypothesize that the NPH may have weakened in response to strong anticyclonic anomalies over the Laurentide Ice Sheet (LIS) but at the same time shifted westward relative to today. Since the NPH is centered over the NE Pacific under present-day conditions, a westward shift would automatically increase the strength of the southerly flow over the NW Pacific. This may explain why the influence of the NPH became stronger over the NW Pacific despite a general weakening of the anticyclone.

Interestingly, the general patterns of temperature change over Beringia and the N Pacific (as inferred from the proxy compilation, Fig. 4c) suggest that the LGM thermal gradient between western and central Beringia and the N Pacific was increased relative to today (Fig. 4c). While warm summers were widespread in western Beringia (Alfimov and Berman, 2001; Kienast, 2002; Kienast et al., 2005; Sher et al., 2005; Berman et al., 2011), the majority of SST records from the open N Pacific and the Bering Sea indicate colder conditions during the LGM (Fig. 4c; de Vernal and Pedersen, 1997; Seki et al., 2009, 2014; Kiefer and Kienast, 2005; Harada et al., 2004, 2012; Maier et al., 2015; Meyer et al., 2016). Under the assumption that alkenone-based reconstructions of LGM SST in the Sea of Okhotsk (Seki et al., 2004, 2009; Harada et al., 2004, 2012) are biased, the Sea of Okhotsk may also have been significantly colder than at present, as suggested by TEX_{86}^L-based SST reconstruction (reduced by ~ 4–$5\,°C$; Seki et al., 2009, 2014). An increased thermal gradient between the subarctic N Pacific and western Beringia would translate into an increased pressure gradient between land and ocean, which would intensify the southerly flow over Kamchatka relative to today. Combined with a weakening of the NPH over the NE Pacific (due to North American ice sheets), this mechanism may have been a potential cause for the westward shift of the NPH.

The distribution of temperature anomalies in the COSMOS simulation shows a different pattern than the proxy compilation (Fig. 4b and c). The model predicts a widespread cooling over Siberia and Kamchatka where the majority of proxy data suggest warmer or equal temperatures relative to present. Relatively warm summers in western and central Beringia (as inferred from the proxy data) have been explained by increased continentality due to the exposure of the Siberian, Bering and Chukchi shelves during the LGM (Guthrie, 2001; Kienast et al., 2005; Berman et al., 2011). In the model the impact of continentality may be comparable to the proxy world over the eastern Siberian and the northern Chukchi shelves since SAT anomalies are between -1 and $+1\,°C$ (Fig. 4b), implying summer SATs similar

to PI conditions. Also, positive anomalies over parts of the Bering and Chukchi shelves are likely associated with the shelf exposure (Fig. 4b). However, for the latter, easterly to southeasterly wind anomalies over southern Alaska and the Bering Land Bridge (Fig. 4b) may also play a role. Given the discrepancies between model and proxies for SAT in the Siberian interior, it seems that the effect of continentality in the COSMOS simulation is weaker than in the proxy world and that other factors are more influential. Reduced CO_{2atm} is a prominent cause for lowered temperature during the LGM (e.g., Kageyama et al., 2006; Shakun et al., 2012). Furthermore, cooling over the Arctic Ocean combined with northerly anomalies in the wind patterns over the eastern Siberian Sea (Fig. 4b) may have enhanced the advection of cold arctic air masses to Siberia, a mechanism supporting SAT decrease in Siberia (Mock et al., 1998). Similarly, northerly anomalies are also present over Kamchatka (Fig. 4a), which are in accordance with summer cooling on the peninsula (Fig. 4a).

Given the discrepancies between proxy-based temperature reconstructions for Siberia and the ESM, the thermal gradient between western Beringia and the subarctic NW Pacific may also differ. In the model simulation the thermal contrast between land and ocean tends to become smaller since the negative temperature anomaly over western Beringia for the most part is more pronounced than over the subarctic N Pacific (Fig. 4b). This contrasts with the proxy compilation, according to which the thermal gradient may have been increased relative to the present gradient (Fig. 4c). As the model predicts a reduction of the thermal gradient the preconditions for the increased landward airflow are not given. In contrast, a reduced thermal gradient would support a northerly anomaly, which is in accordance with the simulated wind patterns over Kamchatka (Fig. 4a). Hence, the discrepancies between proxies and model outputs concerning glacial summer temperature over western Beringia potentially explain the mismatch between model- and proxy-based reconstructions of the atmospheric circulation patterns over the NW Pacific.

5.2.3 The deglaciation (18–10 ka BP)

The deglacial millennial-scale variability resembles the climate development in the N Atlantic as MAT_{ifs} follows the deglacial oscillations recorded in the NGRIP $\delta^{18}O$ (Fig. 2b, i), particularly after ~ 15 ka BP. MAT_{ifs} mirrors the Bølling–Allerød (B–A) interstadial, the Younger Dryas (YD) cold reversal and the subsequent temperature increase into the pre-Boreal (PB; Fig. 2b, i). This similarity to N Atlantic climate change is in line with the majority of SST records from the surrounding seas (Ternois et al., 2000; Seki et al., 2004; Max et al., 2012; Caissie et al., 2010; Praetorius and Mix, 2014; Praetorius et al., 2015; Meyer et al., 2016). This in-phase variability between Greenland and N Pacific records is assumed to result from atmospheric teleconnections be-

tween the N Atlantic and the N Pacific oceans (e.g., Manabe and Stouffer, 1988; Mikolajewicz et al., 1997; Vellinga and Wood, 2002; Okumura et al., 2009; Chikamoto et al., 2012; Max et al., 2012; Kuehn et al., 2014; Praetorius and Mix, 2014). While atmospheric coupling with the N Atlantic seem to have affected Kamchatka between ~ 15 and ~ 10 ka BP, such a connection is questionable during Heinrich Stadial 1 (HS1). The cold spell between ~ 18 and ~ 14.6 ka BP in the MAT_{ifs} record may coincide with the HS1 in the N Atlantic but initiates ~ 2 kyr earlier than in NGRIP $\delta^{18}O$. Therefore, the event in MAT_{ifs} is probably not associated with climate change in the N Atlantic (Fig. 2b, g). This temporal offset cannot be explained by age-model uncertainties in core 12KL since these are in the range of a few hundred years (Max et al., 2012). If the cooling was not associated with climate change in the N Atlantic, it could perhaps represent a local event on Kamchatka, and potentially western Beringia, marking the abrupt end of the warm LGM conditions. Since, to the knowledge of the authors, such an event is not reported in the terrestrial realm of western Beringia, it is difficult to identify the driving processes. One may speculate that the southerly flow abruptly weakened over Kamchatka.

While the western Bering Sea was likely already coupled to the N Atlantic prior to ~ 15 ka BP, the NE Pacific (Praetorius and Mix, 2014) and marginal NW Pacific became linked at ~ 15.5 ka BP (Praetorius and Mix, 2014; Meyer et al., 2016). In the NE Pacific this was explained by a southward shift of the westerly jet over North America (Praetorius and Mix, 2014). In the marginal NW Pacific, accumulation of Alaskan Stream waters likely overprinted the effect of the atmospheric teleconnection by linking the western and the eastern basins of the N Pacific (Meyer et al., 2016). Hence, the effect of the Alaskan Stream may also have determined temperature evolution on Kamchatka during the early deglaciation, which would explain why the linkage to the North Atlantic initiated around 15 ka BP.

The presence of a YD cold reversal on Kamchatka is in agreement with palynological data from the lakes Dolgoe, Smorodynovoye, Ulkhan Chabyda and El'Gygytgyn (Fig. 1a; Pisaric et al., 2001; Anderson et al., 2002; Kokorowski et al., 2008b), suggesting that the N Atlantic climate signal was transmitted to these sites (Kokorowski et al., 2008b). By contrast, a climatic reversal equivalent to the YD is often absent in records from northeast Siberian Lake Jack London, Lake Elikchan 4, Lake El'Gygytgyn and Wrangel Island (Fig. 1a; Lozhkin et al., 1993, 2001, 2007; Lozhkin and Anderson, 1996; Nowaczyk et al., 2002; Nolan et al., 2003; Kokorowski et al., 2008a, b; Andeev et al., 2012). Compiling deglacial records from Beringia, Kokorowski et al. (2008b) identified an east–west gradient across western Beringia with a YD-like climatic reversal being present west of 140° E but absent in records east of 140° E. This east–west gradient was explained by a westward shift of the East Asian Trough (today situated over the Chukchi and Bering shelves; see Fig. 4c; Mock et al., 1998), which caused cooling west

of 140° E by enhancing cold northerly winds, and together with an anticyclone over the Beaufort Sea, brought warming through stronger easterlies into the region east of 140° E (Kokorowski et al., 2008b). The presence of a YD cold reversal on Kamchatka implies that the southeastern edge of Siberia was probably not affected by the shifting East Asian Trough. Several general circulation models investigating the nature of teleconnections between the N Atlantic and N Pacific realms suggest that the westerly jet played an important role by acting as a heat conveyor between the North Atlantic and the North Pacific (e.g., Manabe and Stouffer, 1988; Okumura et al., 2009). Considering the modern average position of the westerly jet (between 30 and 60° N), Kamchatka likely received the YD cold reversal through the westerlies. Together with a shift of the East Asian Trough, (Kokorowski et al., 2008b), this may explain north–south differences in northeastern Siberia.

5.2.4 The Holocene

Although not quite pronounced in magnitude, the long-term MAT_{ifs} evolution during the Holocene is characterized by a HTM between ~ 8 and ~ 4–5 ka BP (Fig. 2b). Since core 12KL shows a relatively poor density of age control points during the Holocene (Fig. 2b), the timing of Holocene climate change has to be interpreted with appropriate caution. Nevertheless, the timing of the HTM is in agreement with existing climate records from central and southern Kamchatka where diatom- and pollen-based records indicate warm and wet conditions between 8 and 5.2 ka BP, which are associated with the HTM (Dirksen et al., 2013; Hoff et al., 2015; Brooks et al., 2015). As already discussed in previous studies, this long-term temperature development is thought to respond to changes in mean summer insolation (Brooks et al., 2015, and references therein).

6 Summary and conclusions

Based on the CBT–MBT′ paleothermometer, a continuous LGM to late Holocene record of summer temperature in Kamchatka is presented.

LGM summers were as warm as at present. The warm summers may result from stronger-than-present southerly winds over Kamchatka as a result of a stronger-than-present anticyclone over the subarctic NW Pacific. The temperature reconstruction as well as the inferences for atmospheric circulation contrast with model simulations, which predict widespread cooling over Siberia and Kamchatka and a weakening of the NPH over the NW Pacific, together with a reduction of southerly winds over Kamchatka. These discrepancies underline the need for further investigations of the LGM climate in the NW Pacific realm using environmental indicators and GCMs.

Abrupt millennial-scale fluctuations characterize the deglacial temperature development and represent the most

prominent changes in summer temperature during the past 20 kyr. A first abrupt cooling event at 18 ka BP marks the end of the warm LGM conditions and was likely caused by regional climate change, the origin of which cannot be identified yet. From around 15 ka onwards, the temperature variations seem to be linked to climate change in the N Atlantic, presumably via atmospheric teleconnections as the B–A interstadial and the YD cold reversal are present. Discrepancies with northeastern Siberian records are possibly related to the position of the westerly jet.

Appendix A

Table A1. Sites and references for the data compiled in Fig. 4c. BLB: Bering Land Bridge.

No.	Site	Region	Proxy	Reference
1	SO201-2-12KL	NW Pacific, Kamchatka	CBT–MBT′	This study
2	SO201-2-12KL	NW Pacific	TEX_{86}^{L}	Meyer et al. (2016)
3	SO201-2-114KL	Western Bering Sea	TEX_{86}^{L}	Meyer et al. (2016)
4	MR0604-PC7	Sea of Okhotsk	$U_{37}^{K'}$	Seki et al. (2009, 2014)
5	XP98-PC2	Sea of Okhotsk	$U_{37}^{K'}$	Seki et al. (2004)
6	XP98-PC4	Sea of Okhotsk	$U_{37}^{K'}$	Seki et al. (2004)
7	MR00K03-PC04	Sea of Okhotsk	$U_{37}^{K'}$	Harada et al. (2004, 2012)
8	Unknown	Sosednee Lake, Siberia	pollen	Lozhkin et al. (1993)
9	Unknown	Oymyakon depression, Siberia	beetle	Berman et al. (2011)
10	Unknown	Middle stream of Indigirka River, Siberia	beetle	Berman et al. (2011)
11	Unknown	Lower and middle reaches Kolyma River, Siberia	beetle	Berman et al. (2011)
12	Mkh	Bykovski Peninsula, Siberia	pollen–beetle	Kienast et al. (2005); Sher et al. (2005)
13	YA02-Tums1	Yana lowlands, Siberia	pollen	Pitul'ko et al. (2007)
14	Unknown	Indigirka Lowland, Siberia	beetle	Alfimov and Berman (2001); Kiselev (1981)
15	Unknown	Kolyma Lowland, Siberia	beetle	Alfimov and Berman (2001); Kiselev (1981)
16	Unknown	Ayon Island, Siberia	beetle	Alfimov and Berman (2001); Kiselev (1981)
17	PG1351	Lake El'Gygytgyn	pollen	Lozhkin et al. (2007)
18	Unknown	Markovo, Siberia	beetle	Alfimov and Berman (2001); Kiselev (1981)
19	Unknown	Anadyr River middle stream, Siberia	beetle	Berman et al. (2011)
20	Bering Shelf 78-15	Shelf off Seward Peninsula, BLB	beetle	Elias et al. (1996, 1997); Elias (2001)
21	Zagoskin Lake	Western Alaska	chironomids	Kurek et al. (2009)
22	Bering Land Bridge National Preserve	Seward Peninsula, Alaska	beetle	Elias (2001)
23	Burial Lake	St. Michael Island, BLB, Alaska	chironomids	Kurek et al. (2009)
24	Bluefish	Bluefish Basin, Alaska	beetle	Matthews Jr. and Telka (1997); Elias (2001)
25	SO202-27-6	Gulf of Alaska	$U_{37}^{K'}$	Maier et al. (2015)
26	PAR87A-10	Gulf of Alaska	dinocysts	de Vernal and Pedersen (1997)
27	MR97-02 St. 8s	NW Pacific	$U_{37}^{K'}$	Harada et al. (2004, 2012)
28	MR98-05 St. 5	NW Pacific	$U_{37}^{K'}$	Harada et al. (2004, 2012)
29	MR98-05 St. 6	NW Pacific	$U_{37}^{K'}$	Harada et al. (2004, 2012)
30	Unknown	Chaun Depression, Siberia	beetle	Berman et al. (2011)

References

Abott, R. J. and Brochmann, C.: History and evolution of the Arctic Flora: in the footsteps of Eric Hultén, Mol. Ecol., 12, 299–313, 2003.

Ager, T. A.: Late Quaternary vegetation and climate history of the central Bering land bridge, St. Michael island, western Alaska, Quaternary Res., 60, 19–32, 2003.

Alder, J. R. and Hostetler, S. W.: Global climate simulations at 3000-year intervals for the last 21 000 years with the GENMOM coupled atmosphere–ocean model, Clim. Past, 11, 449–471, doi:10.5194/cp-11-449-2015, 2015.

Alfimov, A. V. and Berman, D. I.: Beringian climate during the Late Pleistocene and Holocene, Quaternary Sci. Rev., 20, 127–134, doi:10.1016/S0277-3791(00)00128-1, 2001.

Anderson, P. A. and Lozhkin, A. V.: Late Quaternary vegetation of Chukotka (Northeast Russia), implications for Glacial and Holocene environments of Beringia, Quaternary Sci. Rev., 107, 112–128, 2015.

Anderson, P. M., Reanier, R. E., and Brubaker, L. B.: A 14000-year pollen record from Sithylemenkat Lake, north-central Alaska, Quaternary Res., 33, 400–404, 1990.

Anderson, P. M., Lozhkin, A. V., and Brubaker, L. B.: A lacustrine pollen record from North Priokhot'ya: new information about late Quaternary vegetational variations in western Beringia, Arctic Alpine Res., 28, 93–98, 1996.

Anderson, P. M., Lozhkin, A. V., and Brubaker, L. B.: Implications of a 24000-yr palynological record for a Younger Dryas cooling and for boreal forest development in northeastern Siberia, Quaternary Res., 57, 325–333, 2002.

Anderson, P. M., Edwards, M. E., and Brubaker, L. B.: Results and Paleoclimate implications of 35 years of paleoecological research in Alaska, Development in Quaternary Science, 1, 427–440, 2003.

Andreev, A. A., Klimanov, V. A., and Sulerzhitsky, L. D.: Younger Dryas pollen records from central and southern Yakutia, Quaternary Int., 41/42, 111–117, 1997.

Andreev, A. A., Morozova, E., Fedorov, G., Schirrmeister, L., Bobrov, A. A., Kienast, F., and Schwamborn, G.: Vegetation history of central Chukotka deduced from permafrost paleoenvironmental records of the El'gygytgyn Impact Crater, Clim. Past, 8, 1287–1300, doi:10.5194/cp-8-1287-2012, 2012.

Andrén, E., Klimaschewski, A., Self, A. E., Amour, N. St., Andreev, A. A., Bennett, K. D., Conley, D. J., Edwards, T. W. D., Solovieva, N., and Hammarlund, D.: Holocene climate and environmental change in north-eastern Kamchatka (Russian Far East), inferred from a multi-proxy study of lake sediments, Global Planet. Change, 134, 41–54, doi:10.1016/j.gloplacha.2015.02.013, 2015.

Barron, J. A., Heusser, L., Herbert, T., and Lyle, M.: High-resolution climatic evolution of coastal northern California during the past 16,000 years, Paleoceanography, 18, 1020, doi:10.1029/2002PA000768, 2003.

Bartlein, P. J., Anderson, K. H., Anderson, P. M., Edwards, M. E., Mock, C. J., Thompson, R. S., Webb, R. S., Webb, T., and Whitlock, C.: Paleoclimate simulations for North America over the past 21,000 years: Features of the simulated climate and comparisons with paleoenvironmental data, Quaternary Sci. Rev., 17, 549–585, doi:10.1016/S0277-3791(98)00012-2, 1998.

Berger, A. and Loutre, M. F.: Insolation values for the climate of the last 10 million years, Quaternary Sci. Rev., 10, 297–317, 1991.

Berman, D., Alfimov, A., and Kuzmina, S.: Invertebrates of the relict steppe ecosystems of Beringia, and the reconstruction of Pleistocene landscapes, Quaternary Sci. Rev., 30, 2200–2219, doi:10.1016/j.quascirev.2010.09.016, 2011.

Bigelow, N. H. and Edwards, M. E.: A 14000 yr paleoenvironmental record from Windmill Lake, central Alaska: evidence for high-frequency climatic and vegetation fluctuations, Quaternary Sci. Rev., 20, 203–215, 2001.

Bigelow, N. H. and Powers, W. M. R.: Climate, vegetation and archaeology 14 000–9000 cal yr BP in central Alaska, Arctic Anthropol., 38, 171–195, 2001.

Blaga, C. I., Reichart, G.-J., Schouten, S., Lotter, A. F., Werne, J. P., Kosten, S., Mazzeof, N., Lacerot, G., and Sinninghe Damsté, J. S.: Branched glycerol dialkyl glycerol tetraethers in lake sediments: Can they be used as temperature and pH proxies?, Org. Geochem., 41, 1225–1234, doi:10.1016/j.orggeochem.2010.07.002, 2010.

Braconnot, P., Harrison, S. P., Kageyama, M., Bartlein, P. J., Masson-delmotte, V., Abe-ouchi, A., Otto-Bliesner, B., and Zhao, Y.: Evaluation of climate models using palaeoclimatic data, Nature Climate Change, 2, 417–424, doi:10.1038/nclimate1456, 2012.

Brooks, S. J., Diekmann, B., Jones, V. J., and Hammarlund, D.: Holocene environmental change in Kamchatka: A synopsis, Global Planet. Change, 134, 166–174, doi:10.1016/j.gloplacha.2015.09.004, 2015.

Brovkin, V., Raddatz, T., Reick, C., Claussen, M., and Gayler, V.: Global biogeophysical interactions between forest and climate, Geophys. Res. Lett., 36, L07405, doi:10.1029/2009GL037543, 2009.

Brubaker, L. B., Anderson, P. M., and Hu, F. S.: Vegetation ecotone dynamics in southwest Alaska during the late Quaternary, Quaternary Sci. Rev., 20, 175–188, 2001.

Caissie, B. E., Brigham-Grette, J., Lawrence, K. T., Herbert, T. D., and Cook, M. S.: Last Glacial Maximum to Holocene sea surface conditions at Umnak Plateau, Bering Sea, as inferred from diatom, alkenone, and stable isotope records, Paleoceanography, 25, PA1206, doi:10.1029/2008PA001671, 2010.

Chikamoto, M. O., Menviel, L., Abe-Ouchi, A., Ohgaito, R., Timmermann, A., Okazaki, Y., Harada, N., Oka, A., and Mouchet, A.: Variability in North Pacific intermediate and deep water ventilation during Heinrich events in two coupled climate models, Deep-Sea Res. Pt. II, 61–64, 114–126, doi:10.1016/j.dsr2.2011.12.002, 2012.

De Jonge, C., Stadnitskaia, A., Hopmans, E. C., Cherkashov, G., Fedotov, A., and Sinninghe Damsté, J. S.: In situ produced branched glycerol dialkyl glycerol tetraethers in suspended particulate matter from the Yenisei River, Eastern Siberia, Geochim. Cosmochim. Ac., 125, 476–491, doi:10.1016/j.gca.2013.10.031, 2014.

de Vernal, A. and Pedersen, T. F.: Micropaleontology and palynology of core PAR87A-10: A 23,000 year record of paleoenvironmental changes in the Gulf of Alaska, northeast North Pacific, Paleoceanography, 12, 821–830, doi:10.1029/97PA02167, 1997.

Dirksen, V., Dirksen, O., and Diekmann, B.: Holocene vegetation dynamics and climate change in Kamchatka Peninsula, Russian Far East, Rev. Palaeobot. Palynol., 190, 48–65, doi:10.1016/j.revpalbo.2012.11.010, 2013.

Dirksen, V., Dirksen, O., van den Bogaard, C., and Diekmann, B.: Holocene pollen record from Lake Sokoch, interior Kamchatka (Russia), and its paleobotanical and paleoclimatic interpretation, Global Planet. Change, 134, 129–141, doi:10.1016/j.gloplacha.2015.07.010, 2015.

Dong, B. and Valdes, P. J.: Simulations of the Last Glacial Maximum climates using a general circulation model: prescribed versus computed sea surface temperatures, Clim. Dynam., 14, 571–591, 1998.

Dong, L., Li, Q., Li, L., and Zhang, C. L.: Glacial – interglacial contrast in MBT/CBT proxies in the South China Sea: Implications for marine production of branched GDGTs and continental teleconnection, Org. Geochem., 79, 74–82, doi:10.1016/j.orggeochem.2014.12.008, 2015.

Dullo, W. C., Baranov, B., and van den Bogaard, C.: FS Sonne Fahrtbericht/Cruise Report SO201–2, IFM-GEOMAR, Report 35, Kiel, IFM262 GEOMAR, 2009.

Elias, S. and Crocker, B.: The Bering Land Bridge: a moisture barrier to the dispersal of steppe–tundra biota?, Quaternary Sci. Rev., 27, 2473–2483, doi:10.1016/j.quascirev.2008.09.011, 2008.

Elias, S. A.: Mutual climatic range reconstructions of seasonal temperatures based on Late Pleistocene fossil beetle assemblages in Eastern Beringia, Quaternary Sci. Rev., 20, 77–91, doi:10.1016/S0277-3791(00)00130-X, 2001.

Elias, S. A., Short, S. K., Nelson, C. H., and Birks, H. H.: Life and times of the Bering land bridge, Nature, 382, 60–63, doi:10.1038/382060a0, 1996.

Elias, S. A., Short, S. K., and Birks, H. H.: Late Wisconsin environments of the Bering Land Bridge, Palaeogeogr. Palaeocl., 136, 293–308, doi:10.1016/S0031-0182(97)00038-2, 1997.

Fritz, M., Herzschuh, U., Wetterich, S., Lantuit, H., De Pascale, G. P., Pollard, W. H., and Schirrmeister, L.: Late glacial and Holocene sedimentation, vegetation, and climate history from easternmost Beringia (northern Yukon Territory, Canada), Quaternary Res., 78, 549–560, doi:10.1016/j.yqres.2012.07.007, 2012.

Glebova, S., Ustinova, E., and Sorokin, Y.: Long-term changes of atmospheric centers and climate regime of the Okhotsk Sea in the last three decades, PICES Sci. Rep., 36, 3–9, 2009.

Gong, X., Knorr, G., Lohmann, G., and Zhang, X.: Dependence of abrupt Atlantic meridional ocean circulation changes on climate background states, Geophys. Res. Lett., 40, 3698–3704, doi:10.1002/grl.50701, 2013.

Guthrie, R. D.: Origin and causes of the mammoth steppe: a story of cloud cover, woolly mammal tooth pits, buckles, and inside-out Beringia, Quaternary Sci. Rev., 20, 549–574, 2001.

Hammarlund, D., Klimaschewski, A., St. Amour, N. A., Andrén, E., Self, A. E., Solovieva, N., Andreev, A. A., Barnekow, L., and Edwards, T. W. D.: Late Holocene expansion of Siberian dwarf pine (Pinus pumila) in Kamchatka in response to increased snow cover as inferred from lacustrine oxygen-isotope records, Glob. Planet. Change, 134, 91–100, doi:10.1016/j.gloplacha.2015.04.004, 2015.

Harada, N., Ahagon, N., Uchida, M., and Murayama, M.: Northward and southward migrations of frontal zones during the past 40 kyr in the Kuroshio – Oyashio transition area, Geochem. Geophy. Geosys., 5, Q09004, doi:10.1029/2004GC000740, 2004.

Harada, N., Sato, M., Seki, O., Timmermann, A., Moossen, H., Bendle, J., Nakamura, Y., Kimoto, K., Okazaki, Y., Nagashima, K., Gorbarenko, S. A., Ijiri, A., Nakatsuka, T., Menviel, L., Chikamoto, M. O., Abe-Ouchi, A., and Schouten, S.: Sea surface temperature changes in the Okhotsk Sea and adjacent North Pacific during the last glacial maximum and deglaciation, Deep-Sea Res. Pt. II, 61–64, 93–105, doi:10.1016/j.dsr2.2011.12.007, 2012.

Hoff, U., Dirksen, O., Dirksen, V., Kuhn, G., Meyer, H., and Diekmann, B.: Holocene freshwater diatoms: palaeoenvironmental implications from south Kamchatka, Russia, Boreas, 43, 22–41, doi:10.1111/bor.12019, 2014.

Hoff, U., Biskaborn, B. K., Dirksen, V. G., Dirksen, O., Kuhn, G., Meyer, H., Nazarova, L., Roth, A., and Diekmann, B.: Holocene environment of Central Kamchatka, Russia: Implications from a multi-proxy record of Two-Yurts Lake, Global Planet. Change, 134, 101–117, doi:10.1016/j.gloplacha.2015.07.011, 2015.

Hopkins, D. M., Matthews Jr., J. V., Schweger, C. E., and Young, S. B. (Eds.): Paleoecology of Beringia, Academic Press, New York, 1982.

Hopmans, E. C., Schouten, S., Pancost, R. D., Van Der Meer, M. T. J., and Sinninghe Damsté, J. S.: Analysis of intact tetraether lipids in archaeal cell material and sediments by high performance liquid chromatography/atmospheric pressure chemical ionization mass spectrometry, Rapid Commun. Mass Sp., 14, 585–589, 2000.

Hopmans, E. C., Weijers, J. W., Schefuß, E., Herfort, L., Sinninghe Damsté, J. S., and Schouten, S.: A novel proxy for terrestrial organic matter in sediments based on branched and isoprenoid tetraether lipids, Earth Planet. Sc. Lett., 224, 107–116, doi:10.1016/j.epsl.2004.05.012, 2004.

Ivanov, A.: The Far East, in: The Physical Geography of Northern Eurasia, edited by: Shahgedanova, M., Oxford University Press, Oxford, 422–447, 2002.

Jones, V. and Solomina, O.: The Geography of Kamchatka, Global Planet. Change, 134, 3–9, doi:10.1016/j.gloplacha.2015.06.003, 2015.

Jungclaus, J. H., Keenlyside, N., Botzet, M., Haak, H., Luo, J.-J., Latif, M., Marotzke, J., Mikolajewic, M., and Roeckner, E.: Ocean circulation and tropical variability in the coupled model ECHAM5/MPI-OM, J. Climate, 19, 3952–3972, 2006.

Kageyama, M., Laîné, A., Abe-Ouchi, A., Braconnot, P., Cortijo, E., Crucifix, M., de Vernal, A., Guiot, J., Hewitt, C. D., Kitoh, A., Kucera, M., Marti, O., Ohgaito, R., Otto-Bliesner, B., Peltier, W. R., Rosell-Melé, A., Vettoretti, G., Weber, S. L., and Yu, Y.: Last Glacial Maximum temperatures over the North Atlantic, Europe and western Siberia: a comparison between PMIP models, MARGO sea-surface temperatures and pollen-based reconstructions, Quaternary Sci. Rev., 25, 2082–2102, doi:10.1016/j.quascirev.2006.02.010, 2006.

Kageyama, M., Peyron, O., Pinot, S., Tarasov, P., Guiot, J., Joussaume, S., and Ramstein, G.: The Last Glacial Maximum climate over Europe and western Siberia: A PMIP comparison between models and data, Clim. Dynam., 17, 23–43, doi:10.1007/s003820000095, 2001.

Kiefer, T. and Kienast, M.: Patterns of deglacial warming in the Pacific Ocean: a review with emphasis on the time interval of Heinrich event 1, Quaternary Sci. Rev., 24, 1063–1081, doi:10.1016/j.quascirev.2004.02.021, 2005.

Kienast, F.: Die Rekonstruktion der spätquartären Vegetations- und Klimageschichte der Laptewsee-Region auf der Basis botanischer Großrestuntersuchungen, PhD Dissertation, Potsdam University, 116 pp., 2002.

Kienast, F., Schirrmeister, L., Siegert, C., and Tarasov, P.: Palaeobotanical evidence for warm summers in the East Siberian Arctic during the last cold stage, Quaternary Res., 63, 283–300, doi:10.1016/j.yqres.2005.01.003, 2005.

Kim, S. J., Crowley, T. J., Erickson, D. J., Govindasamy, B., Duffy, P. B., and Lee, B. Y.: High-resolution climate simulation of the last glacial maximum, Clim. Dynam., 31, 1–16, doi:10.1007/s00382-007-0332-z, 2008.

Kiselev, S. V.: Beetles in North-East Siberia during the Late Cenozoic, Nauka Press, Moscow, 1981 (in Russian).

Klimaschewski, A., Barnekow, L., Bennett, K. D., Andreev, A. A., Andrén, E., Bobrov, A. A., and Hammarlund, D.: Holocene environmental changes in southern Kamchatka, Far Eastern Russia, inferred from a pollen and testate amoebae peat succession record, Global Planet. Change, 134, 142–154, doi:10.1016/j.gloplacha.2015.09.010, 2015.

Klyuchi climate station: Climate data from Klyuchi climate station, available at: http://en.climate-data.org/location/284590/ (last access: October 2015), 2015.

Knorr, G. and Lohmann, G.: Climate warming during Antarctic ice sheet expansion at the Middle Miocene transition, Nat. Geosci., 7, 376–381, 2014.

Kokorowski, A. H. D., Anderson, P. M., Sletten, R. S., Lozhkin, A. V., and Brown, T. A.: Late Glacial and Early Holocene Climatic Changes Based on a Multiproxy Lacustrine Sediment Record from Northeast Siberia, Arctic,

Antarct. Alp. Res., 40, 497–505, doi:10.1657/1523-0430(07-036)[KOKOROWSKI]2.0.CO;2, 2008a.

Kokorowski, H. D., Anderson, P. M., Mock, C. J., and Lozhkin, A. V.: A re-evaluation and spatial analysis of evidence for a Younger Dryas climatic reversal in Beringia, Quaternary Sci. Rev., 27, 1710–1722, doi:10.1016/j.quascirev.2008.06.010, 2008b.

Kondratyuk, V. I.: Climate of Kamchatka, Hydrometeoizdat, Moscow, 1974 (in Russian).

Kuehn, H., Lembke-Jene, L., Gersonde, R., Esper, O., Lamy, F., Arz, H., Kuhn, G., and Tiedemann, R.: Laminated sediments in the Bering Sea reveal atmospheric teleconnections to Greenland climate on millennial to decadal timescales during the last deglaciation, Clim. Past, 10, 2215–2236, doi:10.5194/cp-10-2215-2014, 2014.

Kurek, J., Cwynar, L. C., Ager, T. A., Abbott, M. B., and Edwards, M. E.: Late Quaternary paleoclimate of western Alaska inferred from fossil chironomids and its relation to vegetation histories, Quaternary Sci. Rev., 28, 799–811, doi:10.1016/j.quascirev.2008.12.001, 2009.

Kutzbach, J., Gallimore, R., Harrison, S., Behling, P., Selin, R., and Laarif, F.: Climate and Biome simulations for the past 21,000 years, Quaternary Sci. Rev., 17, 473–506, 1998.

Kutzbach, J. E. and Wright, E.: Simulation of the climate of 18 000 years BP: results for the North American/North Atlantic/European sector and comparison with the geological record of North America, Quaternary Sci. Rev., 4, 147–185, 1985.

Lohmann, G., Pfeiffer, M., Laepple, T., Leduc, G., and Kim, J.-H.: A model-data comparison of the Holocene global sea surface temperature evolution, Clim. Past, 9, 1807–1839, 2013.

Lozhkin, A. V. and Anderson, P. M.: A late Quaternary pollen record from Elikchan 4 Lake, northeast Siberia, Geol. Pac. Ocean, 12, 609–616, 1996.

Lozhkin, A. V., Anderson, P. M., Ravako, L. G., Hopkins, D. M., Brubaker, L. B., Colinvaux, P. A., and Miller, M. C.: Late Quaternary Lacustrine Pollen Records from Southwestern Beringia, Quaternary Res., 39, 314–324, 1993.

Lozhkin, A. V., Anderson, P. M., Vartanyan, S. L., Brown, T. A., Belaya, B. V., and Kotov, A. N.: Late Quaternary palaeoenvironments and modern pollen data from Wrangel Island (Northern Chukotka), Quaternary Sci. Rev., 20, 217–233, doi:10.1016/S0277-3791(00)00121-9, 2001.

Lozhkin, A. V., Anderson, P. M., Matrosova, T. V., and Minyuk, P. S.: The pollen record from El'gygytgyn Lake: Implications for vegetation and climate histories of northern Chukotka since the late middle Pleistocene, J. Paleolimnol., 37, 135–153, doi:10.1007/s10933-006-9018-5, 2007.

Lund, D. C., Mix, A. C., and Southon, J.: Increased ventilation age of the deep northeast Pacific Ocean during the last deglaciation, Nat. Geosci., 4, 771–774, doi:10.1038/ngeo1272, 2011.

Maier, E., Méheust, M., Abelmann, A., Gersonde, R., Chapligin, B., Ren, J., Stein, R., Meyer, H., and Tiedemann, R.: Deglacial subarctic Pacific surface water hydrography and nutrient dynamics and links to North Atlantic climate variability and atmospheric CO_2, Paleoceanography, 30, 949–968, doi:10.1002/2014PA002763, 2015.

Manabe, S. and Stouffer, R. J.: Two stable equilibria of a coupled ocean-atmosphere model, J. Climate, 1, 841–861, 1988.

Marsland, S. J., Haak, H., Jungclaus, J. H., Latif, M., and Röske, F.: The Max-Planck-Institute global ocean/sea ice model with orthogonal curvilinear coordinates, Ocean Model., 5, 91–127, doi:10.1016/S1463-5003(02)00015-X, 2003.

Mason, O. K., Bowers, P. M., and Hopkins, D. M.: The early Holocene Milankovitch thermal maximum and humans: Adverse conditions for the Denali complex of eastern Beringia, Quaternary Sci. Rev., 20, 525–548, 2001

Matthews Jr., J. V. and Telka, A.: Insect fossils from the Yukon, in: Insects of the Yukon, edited by: Danks, H. V. and Downes, J. A., Ottawa, Biological Survey of Canada (Terrestrial Arthropods), 911–962, 1997.

Max, L., Riethdorf, J.-R., Tiedemann, R., Smirnova, M., Lembke-Jene, L., Fahl, K., Nürnberg, D., Matul, A., and Mollenhauer, G.: Sea surface temperature variability and sea-ice extent in the subarctic northwest Pacific during the past 15,000 years, Paleoceanography, 27, PA3213, doi:10.1029/2012PA002292, 2012.

Meyer, H., Dereviagin, A., Siegert, C., Schirrmeister, L., and Hubberten, H.-W.: Palaeoclimate reconstruction on Big Lyakhovsky Island, north Siberia – Hydrogen and oxygen isotopes in ice wedges, Permafrost Periglac., 13, 91–105, doi:10.1002/ppp.416, 2002.

Meyer, H., Schirrmeister, L., Yoshikawa, K., Opel, T., Wetterich, S., Hubberten, H. W., and Brown, J.: Permafrost evidence for severe winter cooling during the Younger Dryas in northern Alaska, Geophys. Res. Lett., 37, 1–5, doi:10.1029/2009GL041013, 2010.

Meyer, V. D., Max, L., Hefter, J., Tiedemann, R., and Mollenhauer, G.: Glacial-to-Holocene evolution of sea surface temperature and surface circulation in the subarctic northwest Pacific and the Western Bering Sea, Paleoceanography, 31, 916–927, doi:10.1002/2015PA002877, 2016.

Meyer, V. D., Hefter, J., Lohmann, G., Max, L., Tiedemann, R., and Mollenhauer, G.: Fractional abundances and concentrations of branched glycerol dialkyl glycerol tetraethers (brGDGT) of core SO201-2-12KL, doi:10.1594/PANGAEA.870592, 2017.

Mikolajewicz, U., Crowley, T. J., Schiller, A., and Voss, R.: Modelling teleconnections between the North Atlantic and North Pacific during the Younger Dryas, Nature, 387, 384–387, 1997.

Mix, A. C., Bard, E., and Schneider, R.: Environmental processes of the ice age: land, ocean, glaciers (ELIPOG), Quaternary Sci. Rev., 20, 627–657, 2001.

Mock, C. J., Mock, C. J., Bartlein, P. J., Bartlein, P. J., and Anderson, P. A.: Atmospheric circulation patterns and spatial climatic variations, Beringia, Int. J. Climatol., 10, 1085–1104, 1998.

Monnin, E., Indermühle, A., Dällenbach, A., Flückiger, J., Stauffer, B., Stocker, T. F., Raynaud, D., and Barnola, J. M.: Atmospheric CO_2 concentrations over the last glacial termination, Science, 291, 112–114, doi:10.1126/science.291.5501.112, 2001.

Nazarova, L., de Hoog, V., Hoff, U., Dirksen, O., and Diekmann, B.: Late Holocene climate and environmental changes in Kamchatka inferred from the subfossil chironomid record, Quaternary Sci. Rev., 67, 81–92, doi:10.1016/j.quascirev.2013.01.018, 2013.

NGRIP (North Greenland Ice Core Project) members: High-resolution record of northern hemisphere climate extending into the last interglacial period, Nature, 431, 147–151, doi:10.1038/nature02805, 2004.

Nimis, P. L., Malyshev, L. I., Bolognini, G., and Friesen, N.: A multi-variate phytogeographic analysis of plant diversity in the Putorana Plateau (N. Siberia), Opera Bot., 163, 1–72, 1998.

Nolan, M., Liston, G., Prokein, P., Brigham-Grette, J., Sharpton, V. L., and Huntzinger, R.: Analysis of lake ice dynamics and morphology on Lake El'gygytgyn, NE Siberia, Siberia, using synthetic aperture radar (SAR) and Landsat, J. Geophys. Res., 108, 1–12, 2003.

Nowaczyk, N. R., Minyuk, P., Melles, M., Brigham-Grette, J., Glushkova, O., Nolan, M., Lozhkin, A. V., Stetsenko, T. V., Anderson, P. M., and Forman, S. L.: Magneto-stratigraphic results from impact crater Lake El'gygytgyn, northeast Siberia: a 300 kyr long high-resolution terrestrial palaeoclimatic record from the Arctic, Geophys. J. Int., 150, 109–126, 2002.

Okumura, Y. M., Deser, C., Hu, A., Timmermann, A., and Xie, S.-P.: North Pacific Climate Response to Freshwater Forcing in the Subarctic North Atlantic: Oceanic and Atmospheric Pathways, J. Climate, 22, 1424–1445, doi:10.1175/2008JCLI2511.1, 2009.

Parrenin, F., Masson-Delmotte, V., Köhler, P., Raynaud, D., Paillard, D., Schwander, J., Barbante, C., Landais, A., Wegner, A., and Jouzel, J.: Synchronous change of atmospheric CO_2 and Antarctic temperature during the last deglacial warming, Science, 339, 1060–1063, doi:10.1126/science.1226368, 2013.

Peterse, F., Kim, J.-H., Schouten, S., Kristensen, D. K., Koç, N., and Sinninghe Damsté, J. S.: Constraints on the application of the MBT/CBT palaeothermometer at high latitude environments (Svalbard, Norway), Org. Geochem., 40, 692–699, doi:10.1016/j.orggeochem.2009.03.004, 2009.

Peterse, F., van der Meer, J., Schouten, S., Weijers, J. W. H., Fierer, N., Jackson, R. B., Kim, J.-H., and Sinninghe Damsté, J. S.: Revised calibration of the MBT–CBT paleotemperature proxy based on branched tetraether membrane lipids in surface soils, Geochim. Cosmochim. Ac., 96, 215–229, doi:10.1016/j.gca.2012.08.011, 2012.

Peterse, F., Vonk, J., Holmes, M., Giosan, L., Zimov, N., and Eglinton, T. I.: Branched glycerol dialkyl glycerol tetraethers in Arctic lake sediments: Sources and implications for paleothermometry at high latitudes, J. Geophys. Res.-Biogeo., 119, 1738–1754, doi:10.1002/2014JG002639, 2014.

Pisaric, M. F. J., MacDonald, G. M., Velichko, A. A., and Cwynar, L. C.: The late-glacial and post-glacial vegetation history of the northwestern limits of Beringia based on pollen, stomates, and tree stump evidence, Quaternary Sci. Rev., 20, 235–245, 2001.

Pitul'ko, V. V., Pavlova, E. Y., Kuz'mina, S. A., Nikol'skii, P. A., Basilyan, A. E., Tumskoi, V. E., and Anisimov, M. A.: Natural-climatic changes in the Yana-Indigirka lowland during the terminal Kargino time and habitat of late Paleolithic man in northern part of East Siberia, Dokl. Earth Sci., 417, 1256–1260, doi:10.1134/S1028334X07080284, 2007.

Praetorius, S. K. and Mix, A. C.: Synchronization of North Pacific and Greenland climates preceded abrupt deglacial warming, Science, 345, 444–448, doi:10.1126/science.1252000, 2014.

Praetorius, S. K., Mix, A. C., Walczak, M. H., Wolhowe, M. D., Addison, J. A., and Prahl, F. G.: North Pacific deglacial hypoxic events linked to abrupt ocean warming, Nature, 527, 362–366, doi:10.1038/nature15753, 2015.

Raddatz, T. J., Reick, C. H., Knorr, W., Kattge, J., Roeckner, E., Schnur, R., Schnitzler, K.-G., Wetzel, P., and Jungclaus, J.: Will the tropical land biosphere dominate the climate–carbon cycle feedback during the twenty-first century?, Clim. Dynam., 29, 565–574, 2007.

Reimer, P. J., Baillie, M. G., Bard, E., Bayliss, A., Beck, J. W., Blackwell, P. G., Bronk Ramsey, C., Buck, C. E., Burr, G. S., Edwards, R. L., Friedrich, M., Grootes, P. M., Guilderson, T. P., Hajdas, I., Heaton, T. J., Hogg, A. G., Hughen, K. A., Kaiser, K. F., Kromer, B., McCormac, F. G., Manning, S. W., Reimer, R. W., Richards, D. A., Southon, J. R., Talamo, S., Turney, C. S. M., van der Plicht, J., and Weyhenmeyer, C. E.: Intcal09 and marine09 radiocarbon age calibration curves, 0–50,000 years cal BP, Radiocarbon, 51, 1111–1150, 2009.

Roeckner, E., Brokopf, R., Esch, M., Giorgetta, M., Hagemann, S., and Kornbueh, L.: Sensitivity of simulated climate to horizontal and vertical resolution in the ECHAM5 Atmosphere Model, J. Climate, 19, 3771–3791, doi:10.1175/JCLI3824.1, 2006.

Rueda, G., Rosell-Melé, A., Escala, M., Gyllencreutz, R., and Backman, J.: Comparison of instrumental and GDGT-based estimates of sea surface and air temperatures from the Skagerrak, Org. Geochem., 40, 287–291, doi:10.1016/j.orggeochem.2008.10.012, 2009.

Sarnthein, M., Balmer, S., Grootes, P. M., and Mudelsee, M.: Planktic and Benthic ^{14}C Reservoir Ages for Three Ocean Basins, Calibrated by a Suite of ^{14}C Plateaus in the Glacial-to-Deglacial Suigetsu Atmospheric ^{14}C record, Radiocarbon, 57, 129–151, 2015.

Savoskul, O. S.: Holocene glacier advances in the headwaters of Sredniaya Avacha, Kamchatka, Russia, Qual. Res., 52, 14–26, 1999.

Schouten, S., Huguet, C., Hopmans, E. C., and Sinninghe Damsté, J. S.: Improved analytical methodology of the TEX$_{86}$ paleothermometry by high performance liquid chromatography/atmospheric pressure chemical ionization-mass spectrometry, Anal. Chem., 79, 2940–2944, 2007.

Seki, O., Kawamura, K., Ikehara, M., Nakatsuka, T., and Oba, T.: Variation of alkenone sea surface temperature in the Sea of Okhotsk over the last 85 kyrs, Org. Geochem., 35, 347–354, doi:10.1016/j.orggeochem.2003.10.011, 2004.

Seki, O., Sakamoto, T., Sakai, S., Schouten, S., Hopmans, E. C., Sinninghe Damste, J. S., and Pancost, R. D.: Large changes in seasonal sea ice distribution and productivity in the Sea of Okhotsk during the deglaciations, Geochem. Geophy. Geosy., 10, Q10007, doi:10.1029/2009GC002613, 2009.

Seki, O., Bendle, J. a., Harada, N., Kobayashi, M., Sawada, K., Moossen, H., Inglis, G. N., Nagao, S., and Sakamoto, T.: Assessment and calibration of TEX$_{86}$ paleothermometry in the Sea of Okhotsk and sub-polar North Pacific region: Implications for paleoceanography, Prog. Oceanogr., 126, 254–266, doi:10.1016/j.pocean.2014.04.013, 2014.

Self, A. E., Klimaschewski, A., Solovieva, N., Jones, V. J., Andrén, E., Andreev, A. A., Hammarlund, D., and Brooks, S. J.: The relative influences of climate and volcanic activity on Holocene lake development inferred from a mountain lake in central Kamchatka, Global Planet. Change, 134, 67–81, doi:10.1016/j.gloplacha.2015.06.012, 2015.

Shakun, J. D., Clark, P. U., He, F., Marcott, S. A., Mix, A. C., Liu, Z., Otto-Bliesner, B., Schmittner, A., and Bard, E.: Global warming preceded by increasing carbon dioxide concentrations during the last deglaciation, Nature, 484, 49–54, doi:10.1038/nature10915, 2012.

Shanahan, T. M., Hughen, K. A., and Van Mooy, B. A. S.: Temperature sensitivity of branched and isoprenoid GDGTs in Arctic lakes, Org. Geochem., 64, 119–128, doi:10.1016/j.orggeochem.2013.09.010, 2013.

Sher, A. V., Kuzmina, S. A., Kuznetsova, T. V., and Sulerzhitsky, L. D.: New insights into the Weichselian environment and climate of the East Siberian Arctic, derived from fossil insects, plants, and mammals, Quaternary Sci. Rev., 24, 533–569, doi:10.1016/j.quascirev.2004.09.007, 2005.

Smirnova, M. A., Kazarina, G. K., Matul, A. G., and Max, L.: Diatom Evidence for Paleoclimate Changes in the Northwestern Pacific during the Last 20000 Years, Mar. Geol., 55, 425–431, doi:10.1134/S0001437015030157, 2015.

Solovieva, N., Klimaschewski, A., Self, A. E., Jones, V. J., Andrén, E., Andreev, A. A., Hammarlund., D., Lepskaya, E. V., and Nazarova, L.: The Holocene environmental history of a small coastal lake on the north-eastern Kamchatka Peninsula, Global Planet. Change, 134, 55–66, doi:10.1016/j.gloplacha.2015.06.010, 2015.

Stabeno, P. J. and Reed, R. K.: Circulation in the Bering Sea basin by satellite tracked drifters, J. Phys. Oceanogr., 24, 848–854, 1994.

Stärz, M., Lohmann, G., and Knorr, G.: The effect of a dynamic soil scheme on the climate of the mid-Holocene and the Last Glacial Maximum, Clim. Past, 12, 151–170, doi:10.5194/cp-12-151-2016, 2016.

Stepanek, C. and Lohmann, G.: Modelling mid-Pliocene climate with COSMOS, Geosci. Model Dev., 5, 1221–1243, doi:10.5194/gmd-5-1221-2012, 2012.

Stuiver, M. and Reimer, P. J.: Extended C-14 Data-Base and Revised Calib 3.0 C-14 Age Calibration Program, Radiocarbon, 35, 215–230, 1993.

Ternois, Y. T., Awamura, K. K., Hkouchi, N. O., and Eigwin, L. K.: Alkenone sea surface temperature in the Okhotsk Sea for the last 15 kyr, Geochem. J., 34, 283–293, 2000.

Tierney, J. E., Russell, J. M., Eggermont, H., Hopmans, E. C., Verschuren, D., and Sinninghe Damsté, J. S.: Environmental controls on branched tetraether lipid distributions in tropical East African lake sediments, Geochim. Cosmochim. Ac., 74, 4902–4918, doi:10.1016/j.gca.2010.06.002, 2010.

Vellinga, M. and Wood, R. A.: Global climate impacts of a collapse of the Atlantic thermohaline circulation, Climatic Change, 54, 251–267, doi:10,1023/A:1016168827653, 2002.

Vettoretti, G., Peltier, W. R., and McFarlane, N. A.: Global water balance and atmospheric water vapor transport at last glacial maximum: climate simulations with the Canadian Climate Center for Modelling and Analysis atmospheric general circulation model, Can. J. Earth Sci., 37, 695–723, 2000.

Waelbroeck, C., Paul, A., Kucera, M., Rosell-Melé, A., Weinelt, M., Schneider, R., Mix, a. C., Abelmann, A., Armand, L., Bard, E., Barker, S., Barrows, T. T., Benway, H., Cacho, I., Chen, M.-T., Cortijo, E., Crosta, X., de Vernal, A., Dokken, T., Duprat, J., Elderfield, H., Eynaud, F., Gersonde, R., Hayes, A., Henry, M., Hillaire-Marcel, C., Huang, C.-C., Jansen, E., Juggins, S., Kallel, N., Kiefer, T., Kienast, M., Labeyrie, L., Leclaire, H., Londeix, L., Mangin, S., Matthiessen, J., Marret, F., Meland, M., Morey, A. E., Mulitza, S., Pflaumann, U., Pisias, N. G., Radi, T., Rochon, A., Rohling, E. J., Sbaffi, L., Schäfer-Neth, C., Solignac, S., Spero, H., Tachikawa, K., and Turon, J.-L.: Constraints on the magnitude and patterns of ocean cooling at the Last Glacial Maximum, Nat. Geosci., 2, 127–132, doi:10.1038/ngeo411, 2009.

Weber, M. E., Clark, P. U., Kuhn, G., Timmermann, A., Sprenk, D., Gladstone, R., Zhang, X., Lohmann, G., Menviel, L., Chikamoto, M. O., Friedrich, T., and Ohlwein, C.: Millennial-scale variability in Antarctic ice-sheet discharge during the last deglaciation, Nature, 510, 134–138, doi:10.1038/nature13397, 2014.

Wei, W. and Lohmann, G.: Simulated Atlantic Multidecadal Oscillation during the Holocene, J. Climate, 25, 6989–7002, doi:10.1175/JCLI-D-11-00667.1, 2012.

Wei, W., Lohmann, G., and Dima, M.: Distinct modes of internal variability in the Global Meridional Overturning Circulation associated to the Southern Hemisphere westerly winds, J. Phys. Oceanogr., 42, 785–801, doi:10.1175/JPO-D-11-038.1, 2012.

Weijers, J. W. H., Schouten, S., Hopmans, E. C., Geenevasen, J. A. J., David, O. R. P., Coleman, J. M., Pancost, R. D., and Sinninghe Damsté, J. S.: Membrane lipids of mesophilic anaerobic bacteria thriving in peats have typical archaeal traits, Environ. Microbiol. 8, 648–657, 2006a.

Weijers, J. W. H., Schouten, S., Spaargaren, O. C., and Sinninghe Damsté, J. S.: Occurrence and distribution of tetraether membrane lipids in soils: Implications for the use of the TEX_{86} proxy and the BIT index, Org. Geochem., 37, 1680–1693, doi:10.1016/j.orggeochem.2006.07.018, 2006b.

Weijers, J. W. H., Schouten, S., van den Donker, J. C., Hopmans, E. C., and Sinninghe Damsté, J. S.: Environmental controls on bacterial tetraether membrane lipid distribution in soils, Geochim. Cosmochim. Ac., 71, 703–713, doi:10.1016/j.gca.2006.10.003, 2007.

Yanase, W. and Abe-Ouchi, A.: The LGM surface climate and atmospheric circulation over East Asia and the North Pacific in the PMIP2 coupled model simulations, Clim. Past, 3, 439–451, doi:10.5194/cp-3-439-2007, 2007.

Yanase, W. and Abe-Ouchi, A.: A numerical study on the atmospheric circulation over the midlatitude North Pacific during the last glacial maximum, J. Climate, 23, 135–151, doi:10.1175/2009JCLI3148.1, 2010.

Zell, C., Kim, J.-H., Moreira-Turcq, P., Abril, G., Hopmans, E. C., Bonnet, M.-P., Lima Sobrinho, R., and Sinninghe Damsté, J. S.: Disentangling the origins of branched tetraether lipids and crenarchaeol in the lower Amazon River: Implications for GDGT-based proxies, Limnol. Oceanogr., 58, 343–353, doi:10.4319/lo.2013.58.1.0343, 2013.

Zell, C., Kim, J.-H., Hollander, D., Lorenzoni, L., Baker, P., Silva, C. G., Nittrouer, C., and Sinninghe Damsté, J. S.: Sources and distributions of branched and isoprenoid tetraether lipids on the Amazon shelf and fan: Implications for the use of GDGT-based proxies in marine sediments, Geochim. Cosmochim. Ac., 139, 293–312, doi:10.1016/j.gca.2014.04.038, 2014.

Zhang, X., Lohmann, G., Knorr, G., and Xu, X.: Different ocean states and transient characteristics in Last Glacial Maximum simulations and implications for deglaciation, Clim. Past, 9, 2319–2333, doi:10.5194/cp-9-2319-2013, 2013.

Zhang, X., Lohmann, G., Knorr, G., and Purcell, C.: Abrupt glacial climate shifts controlled by ice sheet changes, Nature, 512, 290–294, doi:10.1038/nature13592, 2014.

Zhu, C., Weijers, J. W. H., Wagner, T., Pan, J.-M., Chen, J.-F., and Pancost, R. D.: Sources and distributions of tetraether lipids in surface sediments across a large river-dominated continental margin, Org. Geochem., 42, 376–386, doi:10.1016/j.orggeochem.2011.02.002, 2011.